Article

Thermo-Energy Performance of Lightweight Steel Framed Constructions: A Case Study

Ligia Moga [1], **Ioan Petran** [2], **Paulo Santos** [3] **and Viorel Ungureanu** [4,*]

1 Department of Civil Engineering and Management, Technical University of Cluj-Napoca, 400027 Cluj-Napoca, Romania; ligia.moga@ccm.utcluj.ro
2 Department of Structures, Technical University of Cluj-Napoca, 400027 Cluj-Napoca, Romania; ioan.petran@dst.utcluj.ro
3 Institute for Sustainability and Innovation in Structural Engineering (ISISE), Department of Civil Engineering, University of Coimbra, 3030-788 Coimbra, Portugal; pfsantos@dec.uc.pt
4 Department of Steel Structures and Structural Mechanics, Politehnica University of Timisoara, 300224 Timisoara, Romania
* Correspondence: viorel.ungureanu@upt.ro

Abstract: The building sector continues to play an essential role in reducing worldwide energy consumption. The reduced consumption is accompanied by stricter regulation for the thermotechnical design of the building envelope. The redefined nearly Zero Energy Building levels that will come into force for each member state will pressure designers to rethink the constructive details so that mandatory levels can be reached, without increasing the construction costs over an optimum level but at the same time reducing greenhouse gas emissions. The paper aims to illustrate the main conclusions obtained in assessing the thermo-energy performance of a steel-framed building representing a holistically designed modular laboratory located in a moderate continental temperate climate, characteristic of the south-eastern part of the Pannonian Depression with some sub-Mediterranean influences. An extensive numerical simulation of the main junctions was performed. The thermal performance was established in terms of the main parameters, the adjusted thermal resistances and global thermal insulation coefficient. Further on, the energy consumption for heating was established, and the associated energy rating was in compliance with the Romanian regulations. A parametric study was done to illustrate the energy performance of the investigated case in the five representative climatic zones from Romania. An important conclusion of the research indicates that an emphasis must be placed on the thermotechnical design of Light Steel Framed solutions against increased thermal bridge areas caused by the steel's high thermal conductivity for all building components to reach nZEB levels. Nevertheless, the results indicate an exemplary behaviour compared to classical solutions, but at the same time, the need for an iterative redesign so that all thermo-energy performance indicators are achieved.

Keywords: LSF constructions; thermal bridging; thermal resistance; thermal transmittance; numerical simulation; thermal performance; energy performance; parametric study; nZEB; energy rating

1. Introduction

The building sector is still one of the largest energy consumers worldwide, responsible for around 40% of the European Union's (EU) energy consumption and 36% of greenhouse gas emissions coming from construction, usage, renovation and demolition phases [1]. Through the help of The Green Deal program, a very ambitious target was set of going carbon-neutral by 2050 [2]. Besides the already mandatory actions imposed by the 2018/844 Energy Performance of Buildings Directive (EPBD) [3] (e.g., reaching nearly Zero Energy Buildings (nZEB) for both new and existing buildings, thus providing healthier buildings, more robust implementation of the Energy Performance Certificate (EPC)), each member state has to present a strategy through the National Energy and Climate Plans (NECP)

for tackling energy consumptions in buildings in the period 2021–2030. The aim consists in reaching the goal of reducing energy consumption by 32.5% by 2030 [4]. Considering that the NECP objectives need to be consolidated for reaching the 2030 targets, a review and revision of the Energy Efficiency Directive (EED) [5] took place hand in hand with several targeted provisions of the EPBD. A proposal for the recast on the EU Directive on energy efficiency was published in 2021 [6], which includes reducing the net greenhouse gas emission by at least 55% by 2030 [7] to become climate-neutral by 2050. At the same time, it proposes higher reductions for primary energy consumption -39%, and final energy consumption −36% by 2030. Therefore, the Green Deal initiatives, the Renovation Wave and the Strategy for Energy Sector Integration represent essential programs in promoting energy efficiency [8].

As it was mentioned by the International Energy Agency (IEA) [9], during 2019, the building sector has deviated from the path towards the Paris agreement objectives. A slowing rate of energy efficiency improvement has been observed since 2015 by the IEA [9]. The final energy consumption grew by 2.2% in 2018, and by 2019 the global energy consumption in the building sector remained at the same level compared to previous years [10], as shown in Figure 1. However, the CO_2 emissions from building operations increased around 38% of the global energy-related CO_2 emissions (see Figure 2), including indirect and direct emissions from non-residential buildings and residential buildings as well as the construction industry [10]. Similar conclusions were highlighted back in 2015 by Ürge-Vorsatz in [11], mentioning that commercial heating and cooling was expected to grow until 2050 with an 84% percentile compared to 2010, while residential heating and cooling with a 79%. It was also concluded that the role of electricity is continuously growing, considering that by 2015 it represented around over half for commercial building energy use. At the same time, in the global electricity consumption, the quantity associated with buildings' operation represents around 55%. Therefore, the building sector should decrease emissions by 6% each year until 2030 to remain on track towards the 2050 objectives [10].
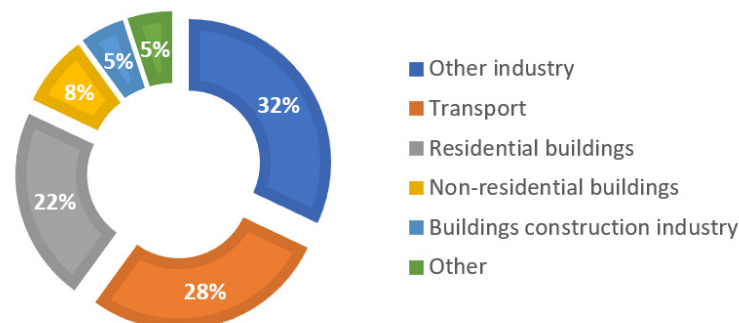

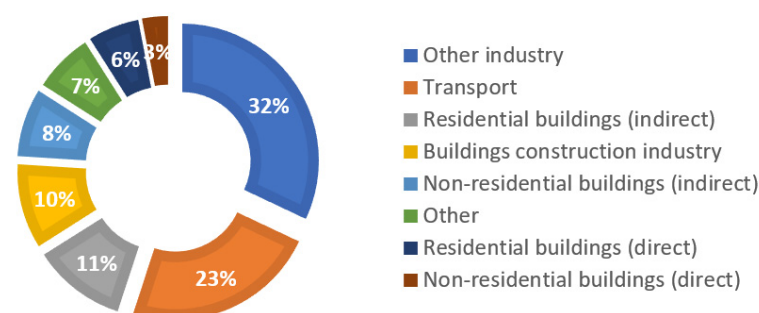**Figure 1.** Global share of buildings and construction final energy, 2019. Adapted from [10].

Figure 2. Global share of buildings and construction final CO_2 emissions 2019. Adapted from [10].

Nevertheless, the global COVID-19 pandemic crisis, along with the housing crisis and the economic crisis, produced disturbances in the building sector. At the same time, the longer the health and economic crisis will last, the greater the impact on buildings' energy

intensity. As mentioned by IEA [9], an estimation was made regarding a decrease in the global energy demand by 5% to 7% due to the global COVID-19 pandemic.

Although the energy efficiency indicators have slowed down on their path, buildings are still the leading sector where investments will be available to keep the direction towards 2050 objectives. Research is done to identify more innovative and feasible approaches to provide sustainable and energy-efficient technical solutions and construction technology.

Considering all the above mentioned, the project CIA_CLIM "Smart buildings adaptable to the climate change effects" [12], aimed to define a prototype solution described by a lightweight steel-framed (LSF) construction that can tackle in the same time energy efficiency and sustainability issues. The achievement of energy-efficient buildings requires an integrated design concerning various factors such as climate, occupant behaviour, technology, operation, and maintenance.

In the energy design of buildings, an important role is defined by how the building envelope can provide the internal comfort conditions resulting from a compliant thermotechnical design. In the case of LSF constructions placed in cold-dominated climates, the need for an accurate design becomes even more critical. Although the number of LSF buildings is increasing around the globe [13,14] due to their advantages compared to heavyweight constructions, the high thermal conductivity of steel elements may lead to significant thermal bridges, which must be well tackled at the design stage to decrease their negative impact on the energy demand for space heating and cooling [15]. Compared to conventional constructive details, the poor thermal performance of the steel elements can be offset by employing adequate thermal insulation solutions. Nevertheless, a significantly increased thickness is needed when conventional thermal insulating materials are used. Thus, an alternative can be the use of nano-insulation materials, also called super insulation materials (SIM), that are defined by a remarkable reduced thermal conductivity (e.g., a thermal conductivity around 15 mW/(m·K) or even lower). As it was demonstrated by Rajanayagam et al. in [15], when using SIMs the same thermal performance will be reached at lower thicknesses compared to conventional thermal insulation materials thicknesses. The paper also demonstrated that the implemented SIM solution was able to reach the imposed building requirements and help address solutions that can be defined by constructive constraints.

Kempton et al. [16] present various solutions for mitigating thermal bridges, starting from slotting the steel frame members to placing sheets of insulation materials or thermal break strips between the steel frame. In this regard, it was proved by Santos et al. in Reference [17] that for steel frames that do not have exterior thermal insulation, the thermal performance can be increased by 16% for one strip of recycled rubber/cork and by 42% in case of two strips placed at opposite sides of the frame. It is worth mentioning that two strips of aerogel were able to mitigate the thermal bridge effect of the steel frame fully. At the same time, in Reference [18], Santos et al. demonstrated the positive impact of the placement of exterior continuous thermal insulation on an LSF wall's overall performance.

Thereby, the objective of our research focused on four directions that aim to provide answers for both designers and builders. First, the paper highlights the thermo-energy performance of the LSF construction, identified as an experimental module. An extensive bidimensional numerical study is presented to evaluate the proposed solutions' thermal bridges and implicitly thermal behaviour. Second, it provides an overview of to what extent this design approach can reach the nZEB levels defined by the Romanian legislation and simultaneously fulfil the European 2030 targets [4]. Thus, the overall energy performance is assessed against the Romanian national regulations [19]. Third, the parametric study results are highlighted to identify the building performance in all representative climatic zones from Romania and their associated energy class for heating. The study includes parametrisation in terms of climatic zone placement, curtain wall orientation, ventilation rate, type of heating system. Fourth, a parametrisation is done to identify to which level the thermal performance of a building envelope component can impact the energy consump-

tion level. Several preliminary conclusions are drawn as a starting point for continuing the research.

2. The Case Study

2.1. Site and Climate

Five climatic zones define the exterior climate of Romania (see Figure 3), starting from the 1st zone with an exterior temperature $\theta_e = -12\,°C$, up to the 5th zone characterised by a $\theta_e = -24\,°C$ [20]. The city of Timișoara is located in the second climatic zone defined by an exterior temperature in the winter period $\theta_e = -15\,°C$. The annual average temperature in Timișoara is 11.4 °C, with an average exterior relative humidity of 72.1% [21]. The coldest winter day is defined by a daily average minimum exterior temperature of −12.6 °C. For the summer period, the average maximum daily exterior temperature is 29 °C.
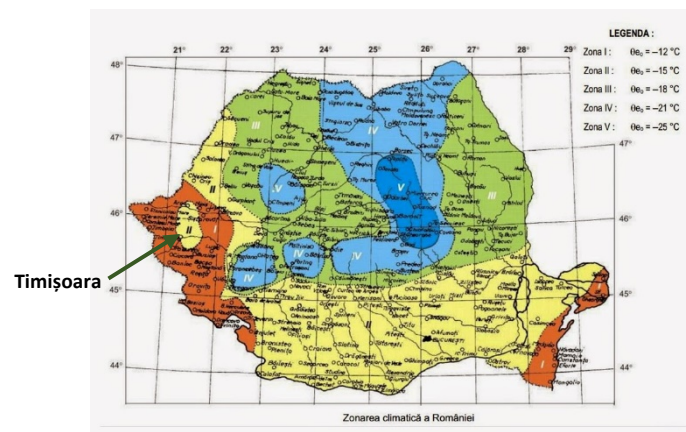

Figure 3. Location of the case study considering the Romanian map for the winter climatic zones. Reprinted from [20].

Buzatu et al. [21] have conducted an analysis with the aim of identifying the impact of Timisoara's climate in terms of internal comfort conditions and energy consumption. The author concluded that according to IWEC weather data and ASHRAE 55 prescriptions in the case of a residential building located in Timişoara at which no design strategies (i.e., heating cooling, natural ventilation or fan-forced ventilation cooling, humidification, dehumidification, shading device, and others) are considered, only 14% (i.e., 1226 h) of the yearly hours are indoor comfortable. Therefore, in order to ensure indoor comfort for a larger period (i.e., over 90% of the annual 8760 h), one must consider several design strategies to provide 7047 h of heating and humidification, along with 387 h cooling and dehumidification (if needed). This leads to a significant increase in the energy demand for the entire year and the building's lifespan. Therefore, integrating several passives and active design strategies for the examined case leads to an annual heating and humidification demand of 4424 h, along with an annual of 31 h for cooling and dehumidification (if needed). That is translated into a reduction of 38% for the annual heating hours and 92% for the annual cooling hours.

One of the passive approaches on which the paper focuses consists of how well the building envelope design can provide proper thermal insulation levels with respect to the thermal performance levels stipulated by design norms [19].

2.2. The Experimental Module

The experimental module, presented in Figures 4 and 5, was designed following sustainability design criteria: material and resources procurement and efficiency, health and well-being, energy and cost-efficiency. Some of the sustainability aspects of LSF constructions include the speed of construction, possibility of prefabrication, architectural flexibility

in building retrofit, small weight with increased mechanical strength, significant potential for recycling and reuse, transportation and handling cost savings, and others [13,22–24].
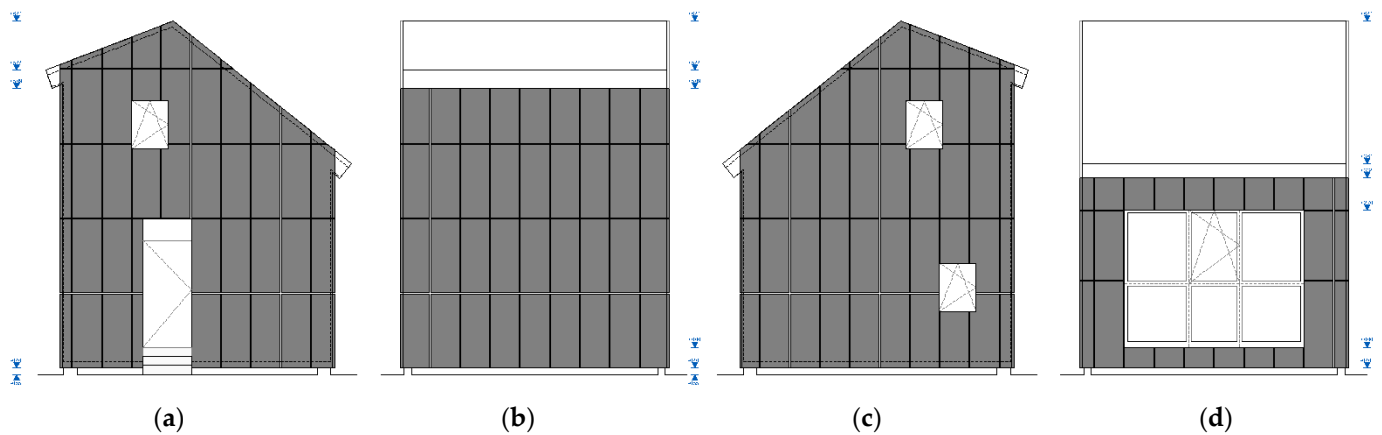

(**a**) (**b**) (**c**) (**d**)

Figure 4. Exterior views of the designed experimental module: (**a**) E orientation; (**b**) N orientation; (**c**) W orientation; (**d**) S orientation.

Figure 5. South view of the built LSF experimental module.

The LSF structure is a two-story modular construction, with a 5 m long span, a 5 m long bay, 3.80 m eave height (on the southern side), and 6.10 m eave height (on the northern side) 6.95 m ridge height (see Figure 4). The eastern façade has two 0.76 m × 0.96 m window openings, the southern façade integrates a 3.56 m × 2.73 m glass curtain opening, while the western façade has a 0.76 m × 0.96 m window opening and a 0.97 m × 2.73 m door opening. There are no openings on the northern side of the building. The access to the second floor is ensured by a 1 m × 1 m attic scuttle door. External photo-voltaic shading lamellae will protect the curtain wall from the sun. The southern side of the roof was designed with a roof pitch of 42° to gain an optimal performance of a roof-mounted solar energy system.

A precast wedge foundation system was adopted, designed as a quick foundation system, easy to handle and install, fully recoverable at the end-of-life of the building and suitable for reuse [25].

Several studies were made to identify the proper materials for the building envelope elements from a holistic design perspective and ease for deconstruction and future reuse of components [26,27]. The chosen thermal insulation is the recycled-PET thermal wadding, fabricated using polyester fibres recycled from post-consumer polyethylene terephthalate

(PET) bottles. This material has a low environmental impact [22,26], high mechanical resistance, and good physical properties [28]. Another reason for this choice was to stimulate the local economy and the recycling and reuse of materials.

Table 1 presents the thermophysical characteristics of the materials used in the LSF experimental module.

Table 1. Thermal properties of the building envelope materials.

Material	Thermal Conductivity [W/(m·K)]	Specific Heat [J/kg·°C]	Density [kg/m^3]
Steel profiles (C150/3, C200/3)	50.00	420	7800
OSB [1]	0.130	1700	620
Recycled-PET [2] thermal wadding	0.054	1350	20
Wood fibreboard	0.050	2100	270
Vapor barrier	0.220	1700	130
Aluminium sheet	160.00	880	2800
XPS [3]	0.035	1450	35
PIR [4] sandwich panel	0.023	1400	30

[1] OSB: oriented strand board; [2] PET: polyethylene terephthalate; [3] XPS: extruded polystyrene; [4] PIR: polyisocyanurate.

The structure is proper for various building envelope configurations. The unidirectional thermal resistances R_{tot} and unidirectional thermal transmittances U_{tot} were calculated based on the constructive details for the envelope components presented in Figure 6. The solutions were chosen with respect to local sourcing and production of building materials, thus reducing transport emissions and associated costs.
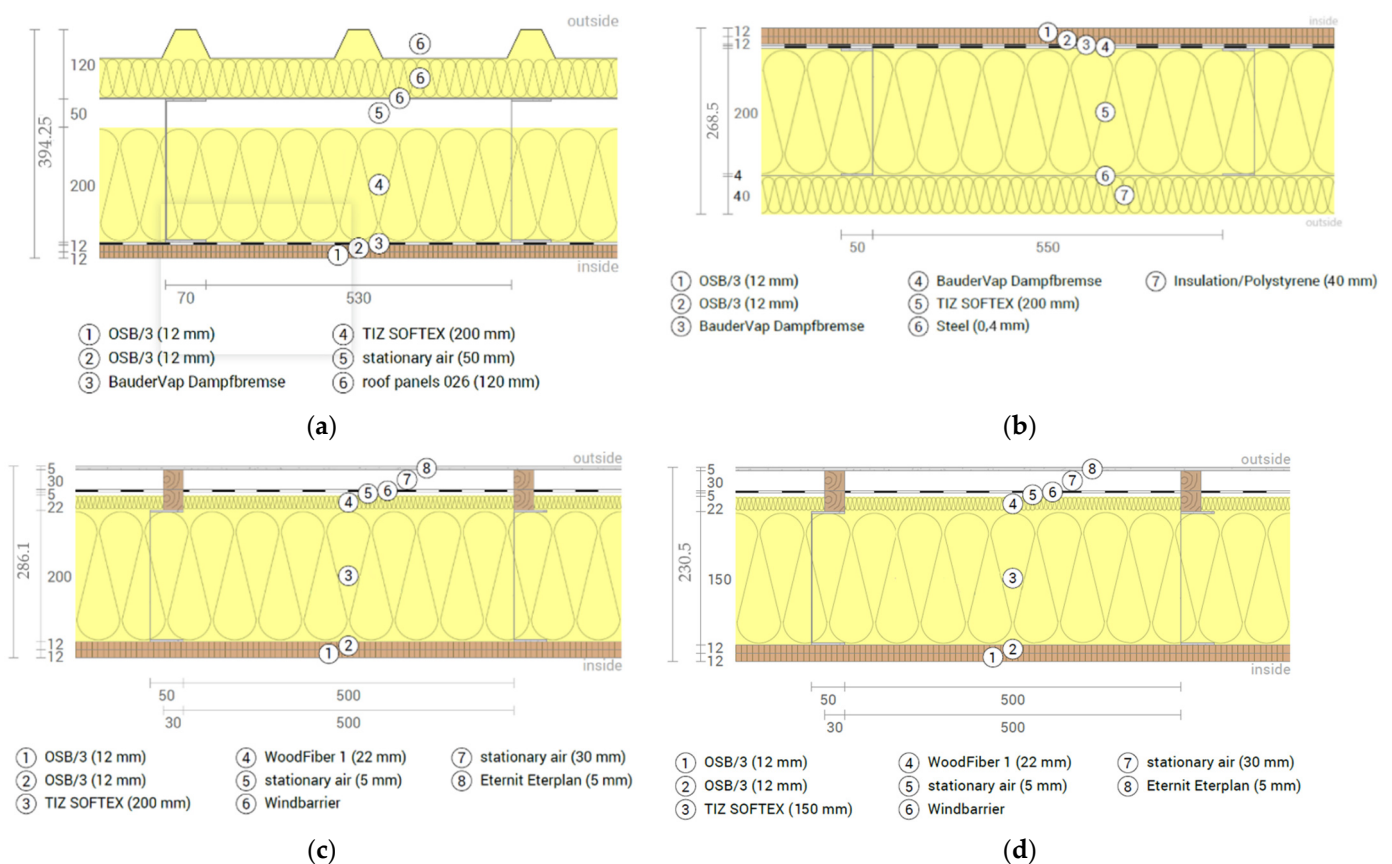

Figure 6. LSF construction elements cross section: (**a**) roof; (**b**) ground floor above crawl space; (**c**) exterior wall north; (**d**) exterior wall—east and west. Reprinted from [22].

An extended presentation of the details from Figure 6 is provided in the next paragraph. Oriented strand board (OSB) panels (24 mm thick) were used as an inner sheeting layer for walls, ceilings and floors. As a thermal insulation material, the recycled-PET thermal wadding was placed between the steel frame, with a thickness of 150 mm, except for the north exterior wall, with 200 mm thick. The exterior wall constructive detail includes a layer of wood fibreboards of 22 mm thick next to the recycled PET thermal wadding, finished by a layer of fiber cement plate of 5 mm thick. The ground floor was elevated 400 mm from the terrain, avoiding moisture retention from the ground. The constructive detail is designed with 200 mm thick recycled PET thermal wadding. A trapezoidal steel sheet of 4 mm thick is placed underneath, and another continuous exterior layer of 40 mm of extruded polystyrene (XPS) closes the element at the exterior bottom side. Polyvinyl chloride (PVC) membranes waterproofed both the floor and roof. The thermal insulation system was completed on the roof in the exterior with PIR sandwich panels of 120 mm thick.

The experimental module was designed following a holistic approach to significantly reduce the energy demand of the building in its operation phase. Therefore, the building envelope design is crucial to meet this objective. At the same time, the design considered the natural light intake and the additional artificial lighting covered by the available LED light sources. The employed renewable energy solutions are based on harvesting solar and wind energy. Therefore, there were installed twelve 250 W polycrystalline cell panels that intake solar energy, with an estimated amount of solar energy produced on-site of 1269 kWh/year (the potential production of the installed polycrystalline cell panels under ideal conditions is 3427.29 kWh/year [26]), and a 1 kW vertical wind turbine.

The LSF experimental module includes a monitoring energy management system that offers a solid overview of the building's performance during the operational phase. The module's functioning is based on the energy provided by the on-site generation technologies, the construction being a non-grid connected building. The data acquisition infrastructure consists of 3 CO_2 sensors, 14 humidity sensors and 53 temperature sensors distributed, as previously presented in reference [22]. Sensors were placed on the inner and outer face of the exterior wall and between the layers.

3. Materials and Methods

3.1. Numerical Approach

It is well known that heat transmission increases significantly through the steel components areas; therefore, even in a thermal insulation layer, the steel element acts as a strong thermal bridge. This phenomenon leads to significant reductions in the global thermal resistance of the building element. Ignoring the negative effect that steel has on the thermal performance of the building envelope can lead to an overestimation of the thermal resistance by up to 50%, as mentioned by Gorgolewski [23]. Simultaneously, the improper temperature profile in the mass of the element can lead to adverse effects, such as condensations and wall staining that occurs on cold spots.

The EN ISO 6946 standard [29] offers the combined method for calculating such constructive details, also known as the simplified method. An upper and lower limit for the thermal resistance is established, also defined as the parallel path and isothermal path method [30]. Based on these two values, their average gives the final thermal resistance. This method is considered to be a simplified one. Other calculation methods were developed based on the presented approach. Nevertheless, an essential prescription of ISO 6946, does not allow the calculation of the thermal performance of a wall with an insulation layer crossed by metal studs due to the increased difference between the upper and lower resistance values which define the combined method.

However, before obtaining the adjusted thermal resistance value R' as defined by the Romanian norms [31], the unidirectional total thermal resistance R_{tot} must be calculated using Equation (1), as prescribed by EN ISO 6946 [26]:

$$R_{tot} = R_{si} + \sum_{j=1}^{n} \frac{d_j}{\lambda_j} + R_{se} \tag{1}$$

where R_{si} and R_{se} are the interior and exterior surface resistances [(m$^2\cdot$K)/W], d is the thickness of a homogenous layer [m] and λ is the thermal conductivity of the material [W/(m$\cdot$K)].

The R_{tot} provides an image of the constructive details' thermal performance that describes the building envelope element without considering the weak thermal areas, i.e., assuming homogeneous layers.

As previously mentioned, each building envelope component is also defined by areas where the heat flow increases due to the significant differences between materials' thermal conductivities. Therefore, the calculations for establishing the adjusted thermal resistance value need to be done at least following a 2D modelling and simulation approach [32], also known as the detailed calculation method. A 3D approach is sometimes mandatory for complex steel junctions to accurately identify the thermal performance [33,34]. Therefore, in order to get an accurate understanding of the thermal performance of the assessed constructive details, extensive numerical modelling and simulation approach was employed, following the prescriptions of the EN ISO 10211 standard [35].

The numerical computation tool used for the analysis is the 2D software called PSI-PLAN [36], which is based on solving the plane heat transfer differential equation in steady-state thermal regime:

$$\frac{\partial}{\partial x} \cdot \left[\lambda(x,y) \cdot \frac{\partial \theta(x,y)}{\partial x} \right] + \frac{\partial}{\partial y} \cdot \left[\lambda(x,y) \cdot \frac{\partial \theta(x,y)}{\partial y} \right] = 0 \tag{2}$$

where θ is the temperature in the node (x,y), and $\lambda(x,y)$ has constant values for the materials describing the detail.

Based on a 2D assessment approach, one can establish the value of the linear heat transfer coefficient defined by ψ [W/(m$\cdot$K)] in order to identify how well from the thermal point of view, the constructive details and implicitly the junction was designed. The coefficient is calculated as described next [35]:

$$\psi = L_{2D} - \sum_{j=1}^{N} U_j \cdot l_j \tag{3}$$

where L_{2D} is the two-dimensional thermal coupling coefficient [W/m$\cdot$K], U_j is the unidirectional thermal transmittance [W/(m$^2\cdot$K)] (i.e., the opposite of R_{tot}) of the component j separating the two environments defined by the internal and external temperature, l_j is the length [m] of the two-dimensional geometrical model over which the U_j value is applied. The ψ value was calculated considering the overall internal dimensions [31].

For the intended research, the ψ value was calculated for each junction as a total value for the assessed junction and also divided in two values, i.e., ψ_1 and ψ_2, each being allocated to one of the modelled wings of the junctions. The need to calculate the two ψ values is following the next calculation steps when the thermal performance of each building envelope element is calculated. This approach is defined in Annex G and Annex J of the Romanian design norm C107/3 [31], which describes the proper approach in reaching the two values. An example of this approach is given in Figure 7.
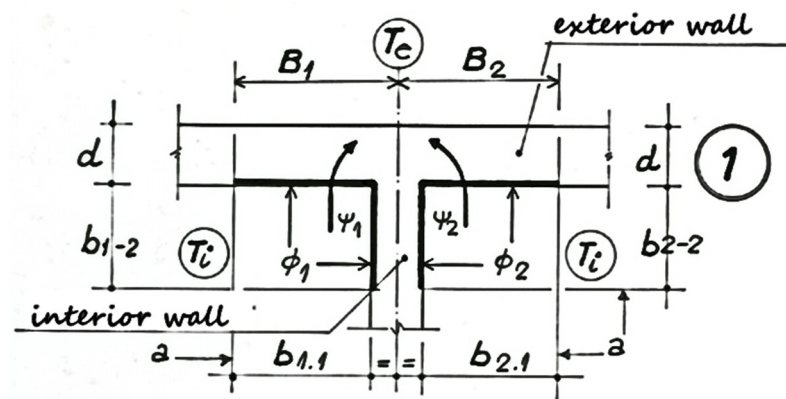
Figure 7. ψ value calculation following the Annex J approach from C107/3. Adapted from [31].

The thermal coupling coefficient L_{2D} is a significant parameter because it shows the heat losses through a building component caused by the temperature difference between the two environments in direct contact with the element. The L_{2D} was obtained based on the heat flow rate ϕ_l [W/m] resulted from the bi-dimensional calculation divided to the temperature difference. The next formula was applied:

$$L_{2D} = \frac{\phi_l}{(\theta_i - \theta_e)} \tag{4}$$

where θ_i is the internal temperature and θ_e the external temperature.

Knowing the ψ value, the adjusted thermal transmittance U' [W/(m²·K)] of the component is calculated [31]. The adjusted value considers all the weak thermal areas of the defined constructive detail by introducing in the calculation formula the ψ values. The Romanian design norms define a minimum imposed value for the adjusted thermal transmittance and the adjusted thermal resistance for each constructive element that defines the building envelope [19]. The minimum imposed values represent one of the design indicators that must be met in designing new buildings and the energy retrofit of the existing ones. The formula for the U' calculations is given next:

$$U' = \frac{1}{R'} = \frac{1}{R_{tot}} + \frac{\sum(\psi \cdot l)}{A} + \frac{\sum \chi}{A} \tag{5}$$

where A is the area of the assessed element of the building envelope [m²], l is the length [m] over which the linear heat transfer coefficient ψ is applied, χ is the point thermal transmittance [W/K] obtained through a 3D simulation, and R_{tot} and ψ were previously defined. The included ψ and χ values are only for the linear and point thermal bridges identified over the A surface of the element. Considering that the approach for the assessed case is 2D, the point thermal transmittance was not considered in calculations. Based on the U' obtained value, the adjusted thermal resistance R' is calculated as an opposite of U'.

The boundary conditions were set for the internal and external environment according to EN ISO 6946 [29]. The surface thermal resistances considered in calculations were $R_{si} = 0.13$ (m²·K)/W, and $R_{se} = 0.04$ (m²·K)/W. The interior temperature considered in calculations was $\theta_i = +20\ °$C, while for the exterior temperature θ_e the studied junctions were modelled in four of the representative climatic zones in Romania starting with a temperature of $\theta_e = -12\ °$C for the 1st climatic zone up to $\theta_e = -21\ °$C for the 4th climatic zone [20,21]. The aim was to identify the temperature distribution variation of the assessed junctions in each of the four climatic zones. Nevertheless, for the calculation of the ψ, R' and U' values in the bi-dimensional numerical simulations, the temperature difference had a unitary value according to ISO 10211 prescription [35].

The data input in the PSIPLAN software is done graphically by using a graphical module. The spatial geometrical and thermotechnical characteristics, the boundary conditions

defined by the superficial thermal resistances, the interior and exterior temperature and relative humidity represent the input data in the program. The meshing of the thermal bridge junction is performed, and with the help of the finite difference method, the temperature values in each node of the discretization network are obtained. The modelling stipulations mentioned in EN ISO 10211 [35] are used.

The program performs the meshing automatically, with respect to the numerical validation as mentioned in Annex C of the Reference [35], point C.2. l that describes the approach for the number of subdivisions and C.2. m that discusses the mandatory convergence value.

As it was previously mentioned in our papers [37–39], the modelling software follows code prescription regarding the calculation of the linear thermal transmittance ψ [W/(m·K)] as well as the design temperature factor at the internal surface f_{Rsi}, also known as the condensation resistance factor [35]:

$$f_{Rsi} = \frac{\theta_{si,min} - \theta_e}{\theta_i - \theta_e} \tag{6}$$

where: $\theta_{si,min}$ is the minimum superficial interior temperature, θ_i is the interior air temperature, and θ_e is the exterior air temperature.

The need to establish the f_{Rsi} value is connected to the aim of identifying the thermal bridge performance. A smaller ψ value indicates a decrease in heat losses and a reduced risk for mold growth, resulting in a higher f_{Rsi} value. Nevertheless, compliance with the mould growth criteria does not necessarily mean a minimized heat flow. Situations are often met in practice when a thermal bridge indicated increased transmission losses, although the values were compliant in terms of mould control.

Based on the obtained results, the global thermal insulation coefficient denoted by G [W/(m³·K)] can be calculated, according to design norm C107 [31]. The G parameter is the first index that provides an overall image of the thermal performance of the building envelope. Therefore, for residential buildings, the following formula is applied:

$$G = \frac{\sum(L_j \cdot \tau_j)}{V} + 0.34 \cdot n \tag{7}$$

where L is the thermal coupling coefficient [W/K], τ_j is the temperature correction coefficient [-], V is the volume of the building envelope [m³], 0.34 is the ratio between the air density and the specific heat of the air at $\theta_i = 20\ °C$ [Wh/(m³·K)], n is the number of air changes per hour due to natural ventilation [h⁻¹] [31]. Its value is compared to the normed value denoted by GN given in reference [19], a value accepted as a maximum for a given case. The reference value for residential buildings is considered in calculations $n = 0.5$ [h⁻¹].

The L thermal coupling coefficient value is calculated for each element of the building envelope component by using the following formula:

$$L = \frac{A}{R'} \tag{8}$$

where A is the area of the element of the building envelope [m²], R' is the adjusted thermal resistance of the building envelope element [(m²·K)/W] calculated as a reversed U' value based on Expression (4). The L value is similar to the transmission heat transfer coefficient H_{tr} coefficient [W/K] that is calculated with the following formula [40],

$$H_{tr} = H_D + H_g + H_u + H_a \tag{9}$$

where H_{tr} is the transmission heat transfer coefficient [W/K], H_D is the direct heat transfer coefficient between the heated or cooled space and the exterior through the building envelope [W/K], H_g transfer coefficient through the ground [W/K], H_u is the transmission

heat transfer coefficient through unconditioned spaces [W/K], H_a is the transmission heat transfer coefficient to adjacent buildings, [W/K].

In the assessed case $L = H_{tr} = H_D$, where H_D is defined by:

$$H_D = \sum_i A_i \cdot U_i + \sum_k l_k \cdot \psi_k + \sum_j \chi_j \tag{10}$$

where all the parameters are the ones previously defined. The only difference between H_D and L is that the summations are done over all the building components separating the internal and the external environments for H_D. In the case of L calculation, the value is calculated per building envelope component, and at the end, all L values are added up for the entire building envelope

The temperature correction coefficient τ_j is calculated by [31]:

$$\tau_j = \frac{\theta_i - \theta_j}{\theta_i - \theta_e} \tag{11}$$

where θ_i is the conventional interior temperature for calculation for each space of the assessed building, while θ_j can either be the exterior temperature or the temperature of the unconditioned interior space. θ_e is the exterior temperature according to the climatic zone, for Timişoara being equal to $-15\,^{\circ}\text{C}$. The aim of τ is to bring a correction for each temperature difference identified for the assessed building by dividing it to the predominant temperature difference described by $(\theta_i - \theta_e)$. Thus, the total coupling coefficient H_{tr} can be multiplied with the predominant temperature difference to obtain the total heat transmission as described in Equation (12). The τ coefficient is similar to the b coefficient as described by ISO 52010-1 [41].

Further on, one can calculate $Q_{H;tr}$ [kWh] as given in ISO 52010-1 [41], describing the total heat transfer by transmission through the building envelope, as described below:

$$Q_{H;tr} = H_{H;tr} \cdot (\theta_{int,calc,H} - \theta_e) \cdot t \tag{12}$$

where $\theta_{int;calc;H}$ is the calculation temperature of the zone for heating [$^{\circ}\text{C}$], t is the duration for the entire heating period, in [h].

The total heat transfer by ventilation $Q_{H;ve}$ [kWh] and the total heat gains $Q_{H,gn}$ described by the solar and internal gains are calculated following reference [42]. The energy need for heating is calculated using Equation (13), as it follows:

$$Q_{H;nd} = Q_{H;ht} - \eta_{H;gn} \cdot Q_{H;gn} \tag{13}$$

where $Q_{H;nd}$ is the energy need for heating defined by the sum of $Q_{H;tr}$ and $Q_{H;ve}$ [kWh], $\eta_{H;gn}$ is the dimensionless gain utilization factor [-].

The energy consumption for heating from heat delivery to heat production as well the energy rating is established based on Equation (14) and the energy scale for heating (i.e., as defined by the Romanian norm) [43]:

$$q_{heat} = \frac{Q_{H;nd}}{\eta \cdot A_u} \tag{14}$$

where η is the efficiency of the heating systems [-], A_u is the useful heated area of the building [m^2]. The heating system's efficiency takes into account losses from heat delivery, regulation, temperature layers, and heat distribution.

3.2. Modelled Cases

To evaluate the thermal performance of the building envelope elements, the representative junctions in the layouts and vertical sections of the building needed to be identified.

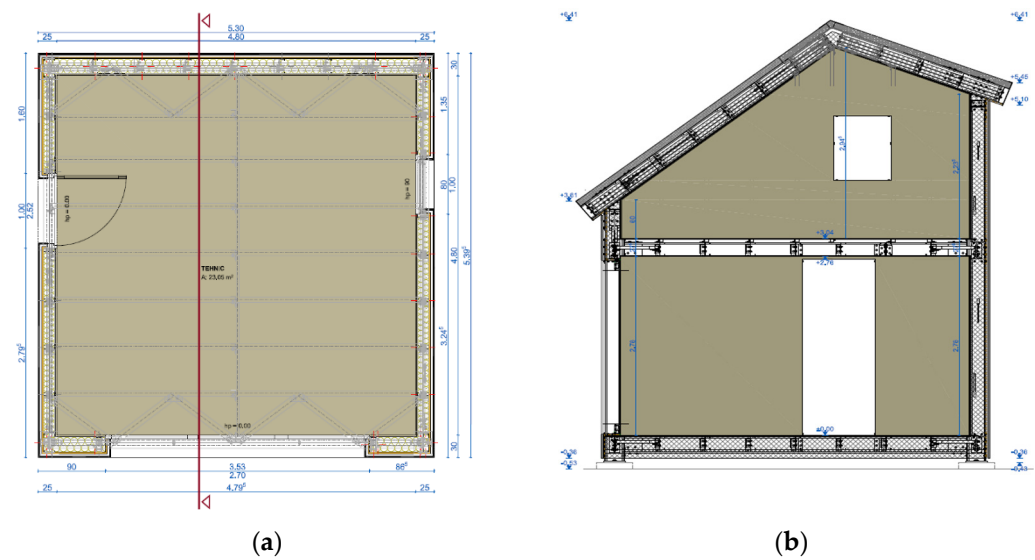Figure 8 provides a detailed image of the building envelope components in layout and cross-sectional view.

(**a**)　　　　　　　　　　　　　　　　(**b**)

Figure 8. Detailed view of the building envelope: (**a**) ground floor layout; (**b**) vertical cross-section.

Based on them, the more thermally permeable junctions were identified, as illustrated in Figure 9. The main constructive details were defined, and the geometrical models were created following each layer and component, their dimensions and thermal conductivities. At the same time, the modelling lengths, as well as the boundary conditions, were set.

(**a**)　　　　　　　　　　　　　　　　(**b**)

Figure 9. *Cont.*

(**c**)   (**d**)
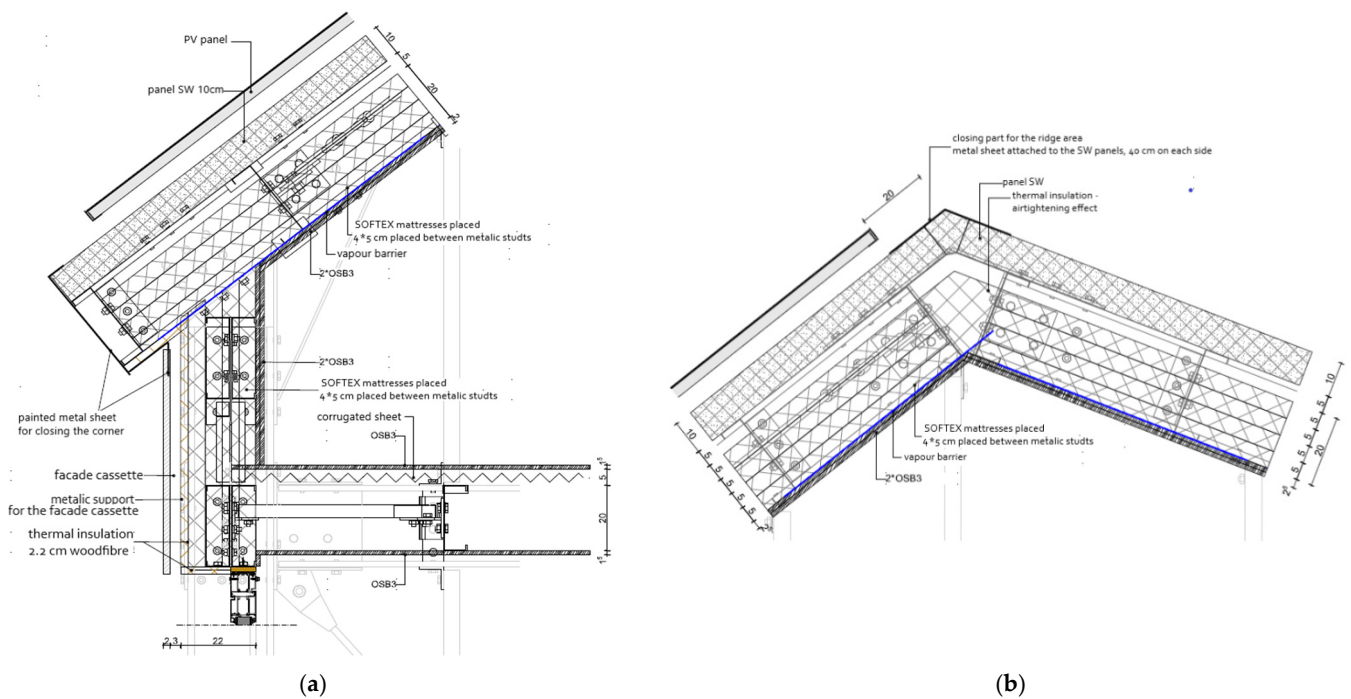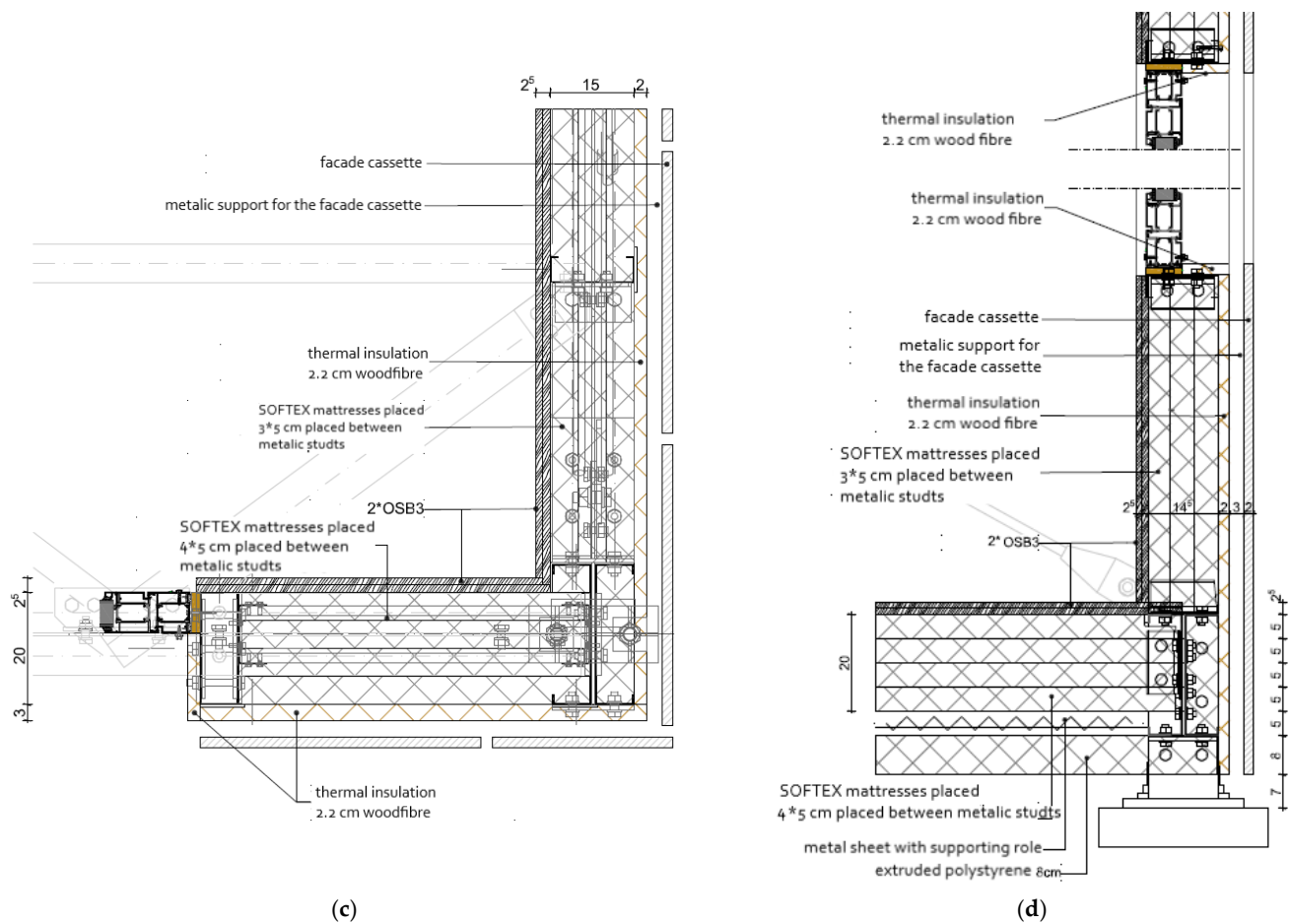
Figure 9. Constructive details at junctions: (**a**) Roof—exterior wall-intermediate floor; (**b**) Ridge zone; (**c**) Exterior corner—window connection, (**d**) Exterior wall—floor in contact with the exterior.

4. Results and Discussion

4.1. Thermal Performance per Element

Table 2 displays the LSF building envelope elements, such as materials, thicknesses, number of layers. The thermal conductivities for each material layer are given in Table 1. The adjusted thermal resistance and adjusted thermal transmittance were calculated at an intermediate stage of development of the CIA_CLIM project [12] using simplified preliminary calculations as provided by the Ubakus tool [42]. The considered constructive details are presented in Figure 6.

Table 2. Materials, thicknesses (d), adjusted thermal resistance (R') and adjusted thermal transmittances (U').

Element	Material Layers (from Inside to Outside)	d [mm]	R'-Value [(m^2·K)/W]	U'-Value [W/(m^2·K)]
Ground floor above the crawl space	OSB	24	3.677	0.272
	Recycled-PET thermal wadding TIZ SOFTEX	200		
	Steel sheet	4		
	XPS	40		
	Total thickness	268.5		

Table 2. *Cont.*

Element	Material Layers (from Inside to Outside)	d [mm]	R'-Value [(m²·K)/W]	U'-Value [W/(m²·K)]
Exterior walls (north)	OSB	24	3.185	0.314
	Recycled-PET thermal wadding-TIZ SOFTEX	200		
	Wood fibreboard	22		
	Stationary air	5		
	Wind barrier			
	Rear ventilated level (outside air)	30		
	Fiber cement plate	5		
	Total thickness	286.1		
Exterior walls (east and west)	OSB	24	2.817	0.355
	Recycled-PET thermal wadding TIZ SOFTEX	150		
	Wood fibreboard	22		
	Stationary air	5		
	Wind barrier			
	Rear ventilated level (outside air)	30		
	Fiber cement plate	5		
	Total thickness	230.5		
Roof	OSB	24	5.208	0.192
	Recycled-PET thermal wadding TIZ SOFTEX	200		
	Stationary air	50		
	PIR sandwich panel	120		
	Total thickness	394.25		
Door and windows	Glass with argon filling	24	1.136	0.880
	PVC casement	92		
Glass Curtain	Glass with argon filling	44	1.351	0.740
	PVC casement	92		

A second analysis included the 2D comprehensive numerical approach. The results are the unidirectional thermal resistance R_{tot}, adjusted thermal resistance R', adjusted thermal transmittance U', the linear thermal transmittance ψ, and the temperature factor f_{Rsi}. The results for the 2D approach using PSIPLAN software are listed in Table 3 for all the analysed junctions. The modelled and simulated results are presented in Figures A1–A8 in the Appendix A.

As mentioned in Section 3.1, the adjusted thermal resistance R', adjusted thermal transmittance U', the linear thermal transmittance ψ and the temperature factor f_{Rsi} were also calculated for each wing, especially for the junction defined by two different building envelope components. The results per modelled wing are presented in Table 4.

As one can see in Tables 3 and 4, the adjusted values per element vary according to the length of the modelled case and modelled wing, constructive detail and position in the building envelope. Starting from 2022, a design requirement that will come into force is that the average ψ value for the building envelope must meet the design criteria $\psi_m \leq 0.15$ W/(m·K) as described in Reference [44]. In this regard, all assessed junctions meet the design criteria with one exception for the Roof eaves—exterior wall intersection. Nevertheless, the average result for ψ_m is met for the building envelope. However, although the reference value was met, it does not implicitly ensure the recommended adjusted thermal resistance.

Table 3. Modelled and simulated junctions-results for the entire length of the modelled cases.

Modelled Cases	R_{tot}-Value [(m²·K)/W]	R'-Value [(m²·K)/W]	U'-Value [W/(m²·K)]	ψ-Value [W/(m·K)]	f_{Rsi}-Value [-]
Exterior wall current field (east and west)	3.660	2.637	0.379	0.066	0.802
Exterior walls current field (north)	4.586	2.981	0.335	0.073	0.823
Exterior corner	4.071	2.059	0.486	0.120	0.690
South Exterior wall-curtain wall left margin	4.586	1.748	0.572	0.136	0.827
South Exterior wall-curtain wall right margin	4.586	1.6542	0.218	0.148	0.826
Exterior wall-window	3.660	1.841	0.543	0.104	0.796
Curtain glass—Ground floor above the crawl space	2.053	1.714	0.583	0.072	0.748
Exterior wall (E,W)—Ground floor above the crawl space	4.584	2.817	0.355	0.082	0.807
Exterior wall (N)—Ground floor above the crawl space	5.247	3.140	0.319	0.077	0.822
Ground floor above the crawl space—current field	6.453	3.951	0.253	0.034	0.918
Exterior wall (E,W)—intermediate floor	3.660	2.476	0.404	0.101	0.922
Exterior wall (N)—intermediate floor	4.586	3.454	0.290	0.055	0.945
Roof—current field	7.987	5.924	0.169	0.0216	0.953
Roof ridge	7.987	3.981	0.251	0.086	0.943
Roof eaves—exterior wall	5.621	2.845	0.351	0.170	0.938

Table 4. Modelled and simulated junctions-results obtained separately per wing of the modelled junctions.

Modelled Cases	Subdivisions	R_{tot}-Value [(m²·K)/W]	R'-Value [(m²·K)/W]	U'-Value [W/(m²·K)]	ψ-Value [W/(m·K)]	f_{Rsi}-Value [-]
Curtain glass—Ground floor above the crawl space	Curtain glass wall	1.351	1.384	0.723	−0.007	0.748
	Ground floor above the crawl space	6.132	2.467	0.405	0.079	0.636
Exterior wall (E,W)—Ground floor above the crawl space	Exterior wall (E,W)	3.660	2.510	0.398	0.038	0.807
	Ground floor above the crawl space	6.132	3.211	0.311	0.045	0.777
Exterior wall (N)—Ground floor above the crawl space	Exterior wall (N)	4.586	2.897	0.345	0.038	0.794
	Ground floor above the crawl space	6.132	3.426	0.292	0.039	0.822
Roof eaves—exterior wall	Roof eaves	7.987	2.510	0.398	0.116	0.895
	Exterior wall	4.586	3.167	0.316	0.054	0.938

Therefore, using the ψ values for each element, Equation (5) and the unidirectional thermal resistances, the final overall adjusted thermal resistances R' for each building envelope element was calculated.

Figure 10 offers an overview of the obtained results, the final R' per building envelope element and the range of R' for the modelled cases, plotted against the normed values for residential buildings according to reference [19]; i.e., exterior walls R'_{min} = 1.80 (m²·K)/W, roof R'_{min} = 5.00 (m²·K)/W, the ground floor above the crawl space R'_{min} = 4.50 (m²·K)/W. As it can be observed, although the range of $R'_{modelled}$ obtained values has a greater domain for each element, the final R' results are achieved just for the exterior wall. In the case of glazing surfaces, the R'_{min} = 0.77 (m²·K)/W is satisfied by the curtain wall, the windows and the door. Regardless of each element's significantly high thermal resistance in its current field, due to the complexity of the details that include steel joining components

and the thermal interaction between different elements, a reduction effect of the thermal performance is obtained.
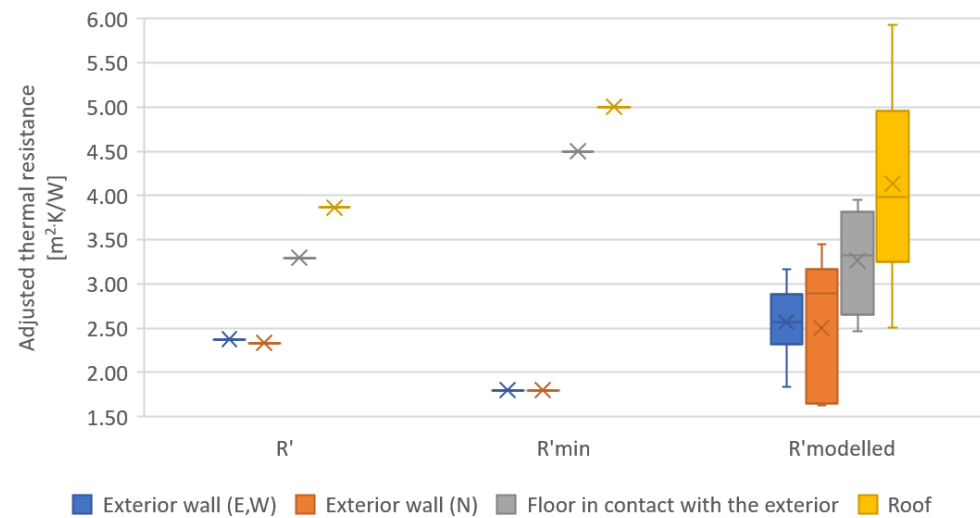

Figure 10. Adjusted thermal resistance comparison: opaque elements.

In the light of reaching the new nZEB criteria that will come into force in Romania starting with 2022 [44], and the increase in the proposed R' values, the design approach must be focused on reaching a unidirectional thermal resistance of at least a $R = 10$ (m^2·K)/W for horizontal or inclined elements and a $R = 7$ (m^2·K)/W for the exterior walls. In this way, after applying the linear and point heat transfer coefficients, the imposed R' values, respectively U' values, are met. A significant increase in the unidirectional thermal resistance value can be reached by thicker thermal insulation or by using super insulating materials, i.e., vacuum insulation panels and aerogel insulation [45–47], preponderantly recommended for LSF buildings.

Regarding the f_{Rsi} factor, the value is considered respected when the one obtained from calculations is greater or equal to a set value [48].

$$f_{Rsi} \geq f_{Rsi,limit} \tag{15}$$

Design criteria may vary from country to country but, in general, a lower limiting value of 0.7 is accepted for the temperature factor to reduce the risk of mould and condensation growth in buildings. Thus, for Romania, a $f_{Rsi,limit} = 0.7$ is considered as the limit value. For the analysed building, values smaller than 0.7 are identified for the floor in contact with the exterior—curtain wall joining and for the case of the exterior corner. Therefore, a thermal redesign of the two junctions could lead to a value greater than 0.7.

4.2. Thermal Performance of the Building Envelope

The thermal coupling coefficient value per element, computed as previously described in Equation (8), is presented in Table 5. The final results per building envelope are indicated in Table 6. Considering the primary function of the building, the interior temperature value at $\theta_i = 20\ °C$ and the fact that all elements are in contact with the exterior environment, the calculation hypothesis was $\tau = 1$. The geometric characteristic for each building envelope component was calculated considering the overall internal dimensions.

The R'_m and U'_m, respectively, indicate the average adjusted thermal resistances and average thermal transmittance per building envelope.

Table 5. The thermal coupling coefficient value (*L*) per element *j*.

Type	Building Envelope Element	A_{Total}	R'	$L_j \cdot \tau_j$
		[m^2]	[m^2 K/W]	[W/K]
1	Exterior Wall	76.57	2.36	32.49
2	Roof	27.61	3.86	7.15
3	Ground floor above the crawl space	23.04	3.30	6.99
4	Curtain wall	9.53	1.35	7.06
5	Glazing surfaces	4.92	1.14	4.33

Table 6. The thermal coupling coefficient value per building envelope.

Building Envelope	A_{Total}	R'_m	$L_j \cdot \tau_j$	U'_m
	[m^2]	[m^2 K/W]	[W/K]	[W/m^2 K]
Total B. Env.	141.67	2.69	58.02	0.37

Figure 11 provides a comparison between the heat losses and the surface areas relative to the entire building envelope results. As one can see, the exterior wall is predominant from both Surface (S) and Heat Losses (HL). In the case of the curtain wall, although its area is smaller than the one of the roof and the floor in contact with the exterior environment, the quantity of heat losses is in the same range as the two mentioned elements. The glazing surfaces exhibit the smallest quantity of HL and a smaller surface.
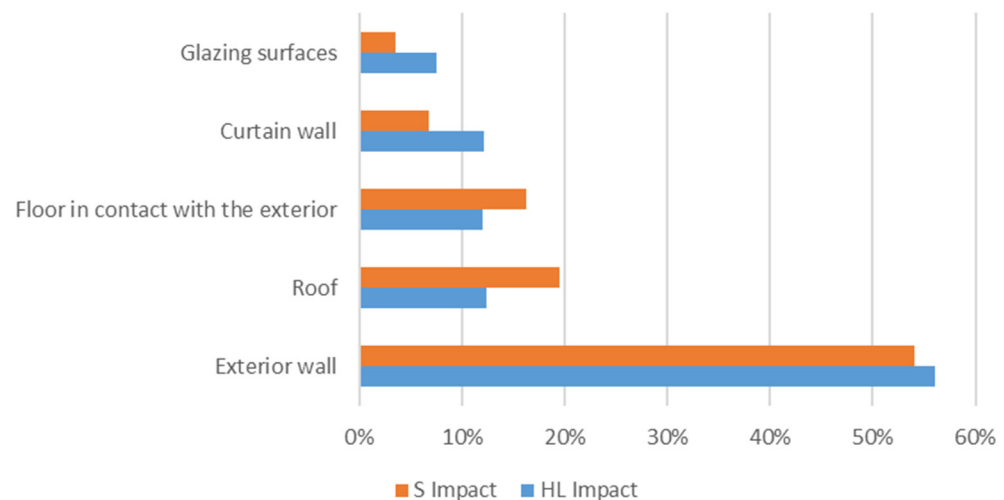
Figure 11. Overview of the Heat Losses (HL) and Surfaces (S) of building envelope elements.

In terms of the global thermal insulation coefficient, the resulting value is $G = 0.661$ W/(m^3·K), where $n = 0.5$ h^{-1} and the volume of building envelope $V = 118.11$ m^3. The resulted value is higher compared to the maximum admissible value $GN = 0.540$ W/(m^3·K) as extracted from [19]. The result follows previous results (i.e., thermal resistance), indicating the necessity of increasing the adjusted thermal resistance for the roof and floor in contact with the exterior at least equal to the normed value. Simultaneously, the results are consistent with the findings from the literature [49,50], mentioning that residential buildings' performance can be highly variable, and even similar houses could have dramatically different performance levels. Nevertheless, as it was mentioned in Reference [22], the building's envelope plays a pivotal role in reducing the energy demand for heating or cooling.

4.3. Energy Performance for Heating of the Building

In terms of energy performance, the energy consumption for heating denoted by q_{heat} is calculated, and an energy rating for heating is established following Equation (14) [43]. After evaluating the heat losses through transmission and the heat losses through venti-

lation, the internal heat gains and the solar gains were established. The heating system's efficiency was considered $\eta = 85\%$ thus resulting in a B energy class for heating (Figure 12) characterized by a $q_{heat} = 110.33$ kWh/(m²·yr). It should be mentioned that the calculations do not consider the overall embodied energy of the building. Therefore, it is highlighted the need to provide energy-efficient solutions [22] described by alternative energy sources to reduce the overall energy consumption.
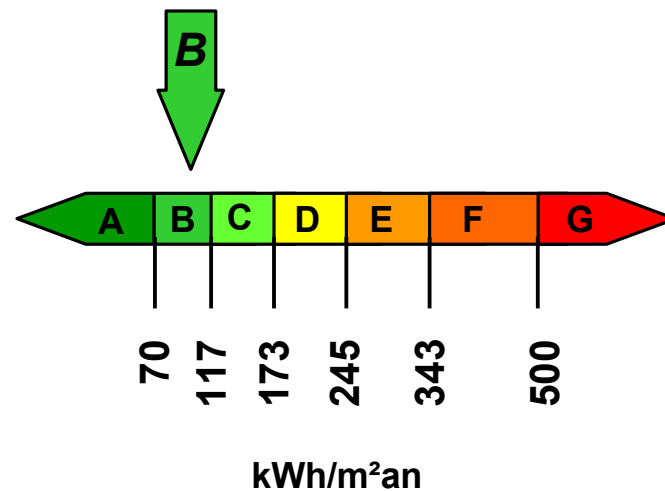
Figure 12. Energy class based on the energy consumption for heating.

4.4. Parametric Study for the Energy Performance for Heating of the Building

In order to offer an image of the energy consumption for heating of the experimental module placed in all five climatic zones from Romania, a parametric study was performed, resulting in 360 case scenarios. The data considered in the study is briefly presented in Table 7.

Table 7. The parametric data for the considered case scenarios.

Parameters	Examined Range
Climatic zone	1st, 2nd, 3rd, 4th and 5th zone
Curtain wall orientation	S, SW, W
Ventilation rate, n [h^{-1}]	0.5, 0.4, 0.3
Heating system efficiency, η [%]	75—Hot-water floor heating system 40°/30 °C 80—Water radiator 70°/40 °C with manifold 82—Electric floor heating 83—Water radiator 45°/35 °C with manifold 86—Roof heating (i.e., electric) 87—Water radiator 70°/40 °C 89—Water radiator 45°/35 °C 95—Electric heater

Due to its larger surface, the curtain wall orientation was considered the main façade from the solar gains perspective. Thus, the other two positions for the main orientation were considered (i.e., SW and W) in order to have a significant solar gain still.

For the ventilation rate n, the chosen reference value was 0.5 as prescribed by the thermotechnical design norm [31] The two other values provided in Table 7 indicate other cases with better control of the ventilation rate and implicitly of the heat losses

For the heating system efficiency, several case scenarios were considered, starting from a $\eta = 75\%$ specific for hot-water floor heating system 40°/30 °C up to a $\eta = 95\%$ that defines the case of an electric heater, as provided by the methodology Mc001 [43].

In terms of *G* value, the smallest result obtained for the studied cases was $G = 0.593$ W/(m^3·K), which is still higher compared to the reference value of $GN = 0.540$ W/(m^3·K).

In terms of energy performance for heating, one can observe in Figure 13 that q_{heat} for all examined cases ranges from a value greater than $q_{heat} = 70$ kWh/(m^2·yr), to one smaller than $q_{heat} = 190$ kWh/(m^2·yr). The extreme values (i.e., smallest and highest) are identified for the 1st climatic zone $q_{heat} = 71.09$ kWh/(m^2·yr), $n = 0.3$ h^{-1}, S orientation, $\eta = 95\%$ and for the 5th climatic zone $q_{heat} = 211.99$ kWh/(m^2·yr), $n = 0.5$ h^{-1}, W orientation, $\eta = 75\%$. Therefore, the energy class for heating ranges from B up to a D class for the experimental module, as illustrated in Table 8. An overview of the assessed case scenarios is also provided in Figure 14.
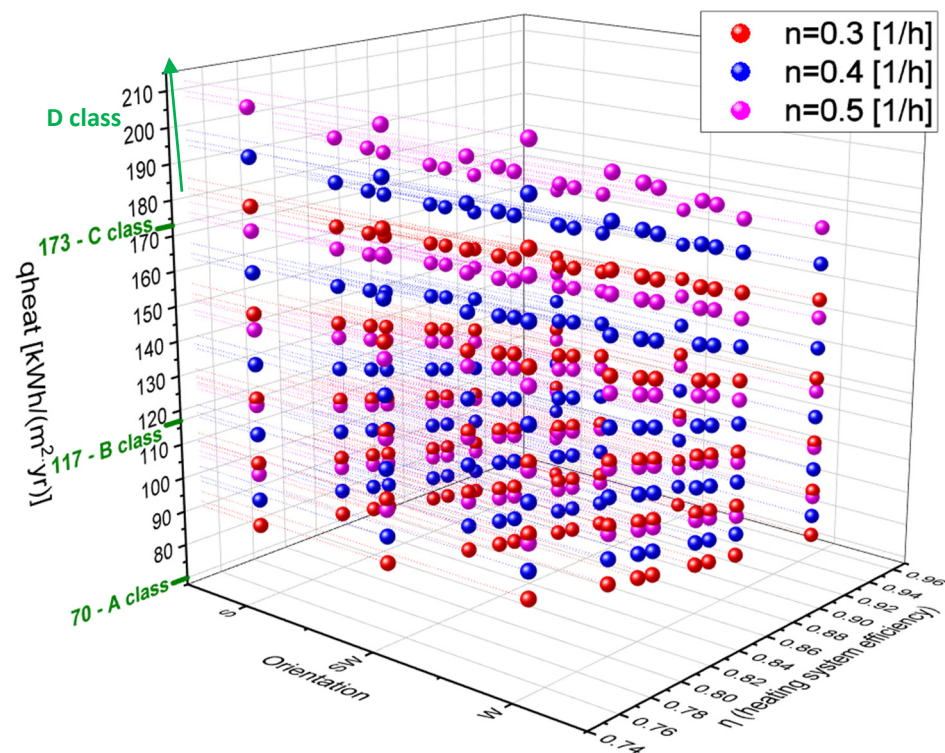
Figure 13. The energy consumption for heating for the 360 case scenarios.

Table 8. Obtained minimum and maximum values for the heating energy consumption, q_{heat}, and corresponding energy class for heating per climatic zone.

Values	q_{heat} [kWh/(m^2·yr)]—Energy Class per Climatic Zone				
	1st	**2nd**	**3rd**	**4th**	**5th**
Minimum	71.09—B	85.46—B	100.17—B	119.21—C	142.77—C
Maximum	109.38—B	128.62—B	150.37—C	178.40—C	211.99—D

As illustrated in Table 8, the 1st and 2nd climatic zone are the most favourable locations for the investigated building in terms of reduced energy consumption for heating. However, the A energy class is still not met.

In terms of the ventilation rate (*n*), the value equal $n = 0.3$ h^{-1} and a heating system efficiency $\eta = 95\%$ which define a best-case scenario for the building, results fall within B and C energy class, respectively $q_{heat} = 71.09$ kWh/(m^2·yr), 1st climatic zone, and $q_{heat} = 142.77$ kWh/(m^2·yr), 5th climatic zone.

(a) Ventilation rate n = 0.3 h^{-1}

(b) Ventilation rate n = 0.4 h^{-1}

(c) Ventilation rate n = 0.5 h^{-1}
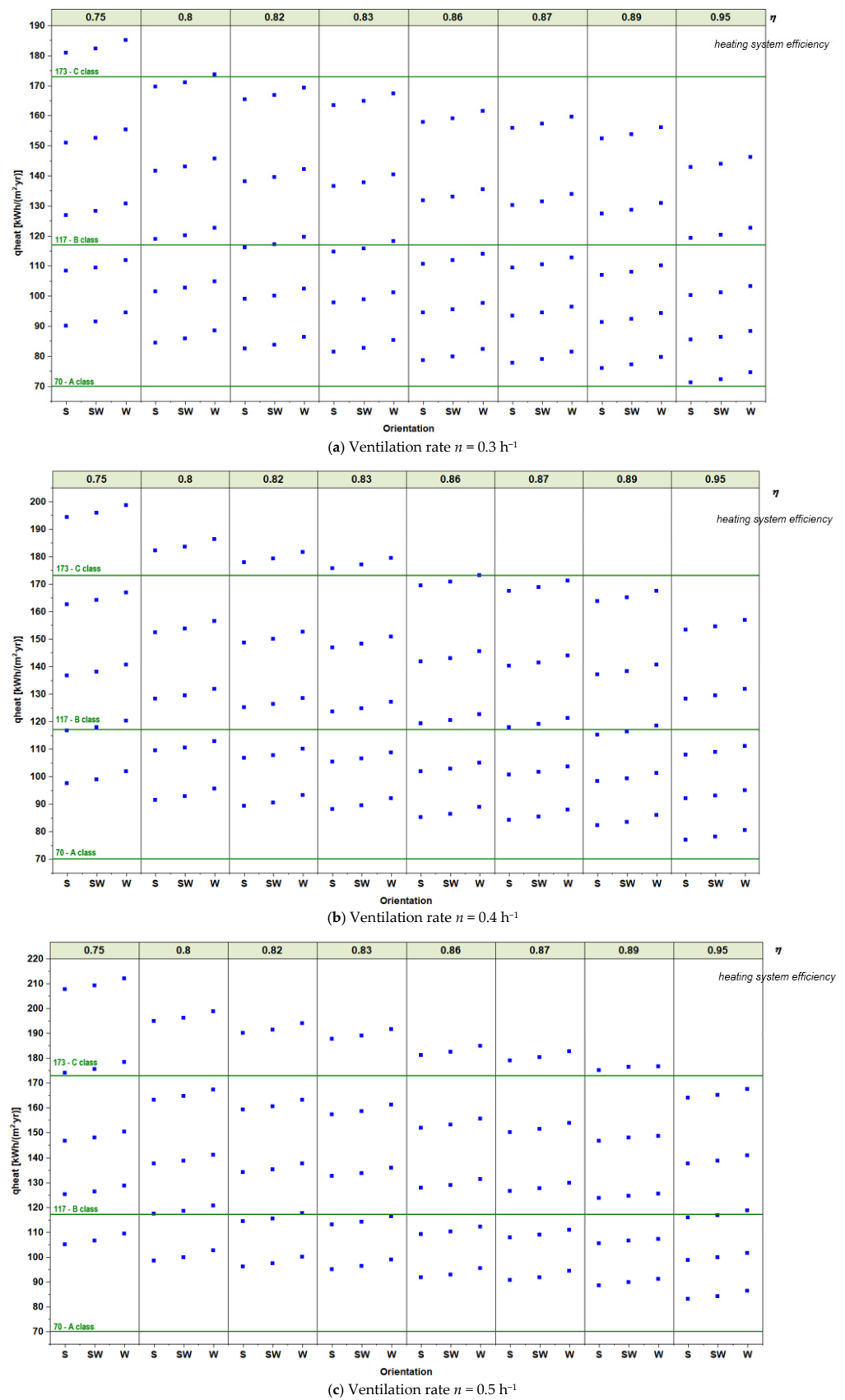
Figure 14. The energy consumption for heating for the case scenario (**a**) n = 0.3 h^{-1}, (**b**) n = 0.4 h^{-1}, (**c**) n = 0.5 h^{-1} for the five climatic zones and for the heating system efficiency raging from η = 75% up to η = 95%.

The South orientation is the most favourable for the considered location and façade design when looking at solar gains. Nevertheless, even for a maximum solar gain for the 5th climatic zone, in the case of a $n = 0.5$ h^{-1} and $\eta = 95\%$, the $q_{heat} = 163.99$ kWh/(m$^2\cdot$yr) corresponds to a C energy class for heating. In contrast, for a poorer heating system efficiency of $\eta = 75\%$, the $q_{heat} = 207.72$ kWh/(m$^2\cdot$yr) describes a D energy class for heating.

In terms of energy consumptions values for the same orientation for all assessed cases per climatic zone, the difference between the worst and the best results is around 21%. When comparing energy consumption in one climatic zone, the results vary between the considered orientations from 1% to 5%. Instead, when considering the results for the 1st climatic zone as the reference values, the increase in the energy consumptions for the same orientation starts from 16% for the 2nd climatic zone to 50% for the 5th climatic zone. Between two consecutive climatic zones for the same orientation, the values vary between 14–16%, while the values vary around 28–29% between every second climatic zone.

Thus, from the obtained results, it is clear that strategy of heat recovery for the assessed building as well as the use of alternative energy sources for energy production will help the building in meeting the existing A class defined range, as well as the upcoming values for A and A+ energy classes for heating as mentioned in Reference [44]. At the same time, the heating energy demand can be significantly reduced by an optimum orientation, in terms of optimising the passive solar gain, of the façade defined by a large glazing area (i.e., windows), a reduced ventilation rate according to the code requirements, and by selecting a heating system having a higher energy efficiency.

4.5. Parametric Study for the Building Envelope Thermal Performance Impact on the Energy Consumption for Heating

As it is previously shown in Table 5, the roof, as well as the ground floor above the crawl space, are underperforming with a direct negative impact on the energy performance consumption and energy rating. A parametrisation was done to assess the impact of each building envelope component on the energy performance in terms of heating. The parametrisation was done for the case described by a South orientation of the curtain-wall, a ventilation rate $n = 0.5$ h^{-1} and a heating system defined by a water radiator $70°/40$ °C with a $\eta = 87\%$. The considered case scenarios and the associated results are presented in Table 9.

Table 9. Results in the parametrisation of R' value for each building envelope component–correlation with the energy consumption for heating q_{heat}.

Type	Building Envelope Element	R' [m^2 K/W]				
		Ref.	(1)	(2)	(3)	(4)
1	Exterior Wall	2.36	2.36	2.36	2.36	*4.00*
2	Roof	3.86	*5.00*	3.86	*5.00*	*6.67*
3	Ground floor above the crawl space	3.30	3.30	*4.50*	*4.50*	*5.00*
4	Curtain wall	1.35	1.35	1.35	1.35	1.35
5	Glazing surfaces	1.14	1.14	1.14	1.14	1.14
	q_{heat} [kWh/(m$^2\cdot$yr)]	107.79	104.70	104.25	101.14	72.12
	Reduction		3%	3%	6%	33%

The reference case scenario provides the resulting values presented in Table 5 for the as-designed and as-built building. The parametrisation does not include variations for the curtain wall and glazing surface due to already met code values. Case scenarios (1), (2) and (3) highlight the change in respect to reaching the code adjusted thermal resistances values. As demonstrated before, the roof and the ground floor above the crawl space illustrate the same thermal performance. Consequently, they display the same reduction when the code value is met, i.e., case 1 and case 2. For case scenario (3), both construction elements meet the code requirements. However, the decrease is still small compared to the reference case and the 4th case scenario, where it was considered that the proposed reference values

R' [44] are met for the opaque construction elements. All four case scenarios provide a B energy class for heating in terms of energy rating. Nevertheless, for some of the assessed case scenarios defined at 4.4, an A energy class for heating could be met for climatic zones 1 and 2 if the proposed code requirements are met.

5. Conclusions

The path toward the decarbonization of the building stock started with the recast of the Energy Performance of Buildings Directive back in 2010 and when the policies for climate and energy for 2020 were defined. This path was defined by short, medium and long-term strategies that should lead us to have an entire building stock up to nearly Zero Energy Buildings levels and even lower. Reaching nZEB levels will generate a reduction in energy consumption that will contribute to the reduction of GHG emissions resulting from the same sector. Positive results are expected from residential and non-residential buildings (i.e., governmental buildings, public buildings, office buildings).

However, achieving buildings with a notable reduced impact on the environment during the operational phase depends on the proper use of the holistic approach from the initial design stages. For the investigated case, in terms of mandatory adjusted thermal resistances (i.e., adjusted thermal transmittances), it can be concluded that the values can be met for typical vertical opaque elements (i.e., exterior walls). In contrast, a thermomechanical redesign is necessary for horizontal or inclined elements.

At the same time, the choice in thermal insulation material must be redirected towards nano-insulation materials. Thus, instead of using 20–30 or even more centimetres of typical thermal insulation, one can use a thinner layer to obtain the same thermal effect. Another aspect that must be considered is preserving the thermal properties of these materials, which might be negatively affected when penetrated by fixing components. The position of the thermal insulation in the constructive detail and the negative impact of the point thermal bridges that shape such structures must also be addressed. Although those LSF buildings indicate a proper thermal performance compared to other existing solutions, more research can be done on the passive measures by which the energy consumption can be reduced in direct correlation with the building envelope design criteria, i.e., shape, orientation, compactness, window to wall ratio, constructive details, ψ and χ magnitude, reduced negative impact caused by the area of the thermal bridge, and others.

Regarding the energy performance for heating, the results are somehow favourable only for 2 of the 5 climatic zones from Romania. However, the experimental module should be redesigned for an A and A+ energy class. Simultaneously, considering the new nZEB criteria that will come into force starting with 2022, iterative calculations will be emphasized so that both the mandatory thermal performance per building envelope element and global energy performance per type of building are achieved.

The novelty of the study lies in the fact that an extensive bidimensional numerical study was carried out to assess the building envelope's junctions. In current design practise, steel structures are assessed by employing unidirectional calculations. The resulting R_{tot} values for each building component are later adjusted by using a predefined reduction coefficient "r" that often does not comply with the assessed performance. In comparison, the bidimensional modelling and simulation of the junction can also provide the thermal interaction between various building components. Also, a comparison is made for the experimental module placed in various climatic zones from Romania. Thus, an image of the energy consumption profile can be illustrated, based on which design conclusions can be highlighted regarding the thermal design of building envelope components, orientation, ventilation rate and heating system efficiency. However, the study's limitations are the lack of experimental validation for the building envelope thermal performance at this stage and the impossibility of assessing all considered case scenarios for the heating system in real operation of the building.

Furthermore, for the examined experimental module, a monitoring phase will provide answers regarding the extent to which the employed alternative systems will impact the

improvement of the total energy performance of the building. The results interpretation will indicate if the LSF prototype solution can comply with the new nZEB energy consumptions levels and the new incoming definition that will set out the nearly Zero Emissions Building.
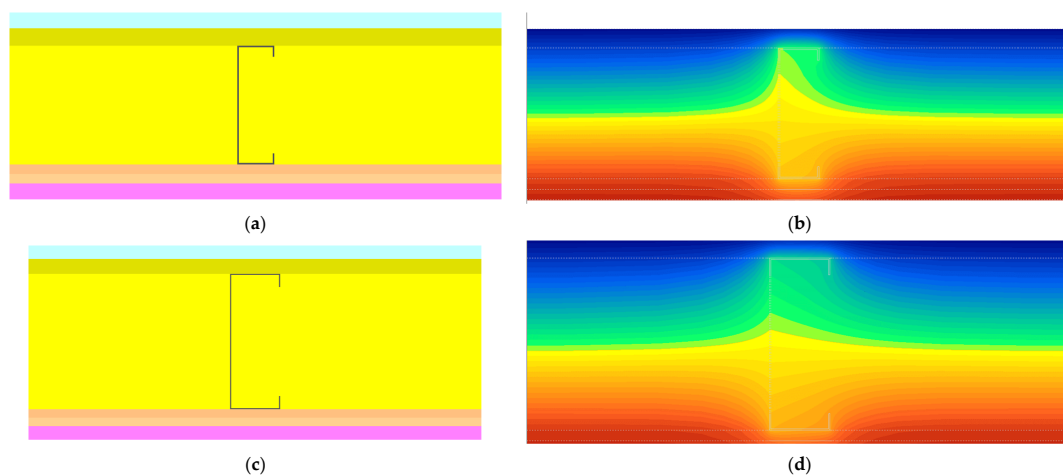
Appendix A

Figure A1. Exterior wall current field-Geometrical models (**a**) east and west, (**c**) north; Isothermal surfaces (**b**) east and west, (**d**) north.
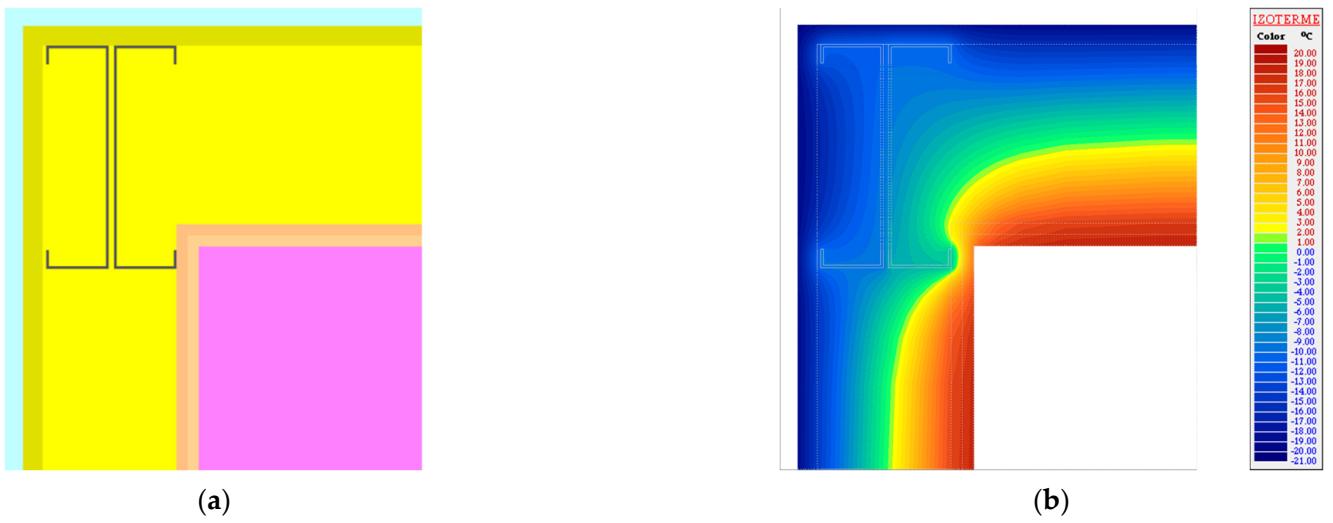
Figure A2. Exterior corner: (**a**) Geometrical models; (**b**) Isothermal surfaces.
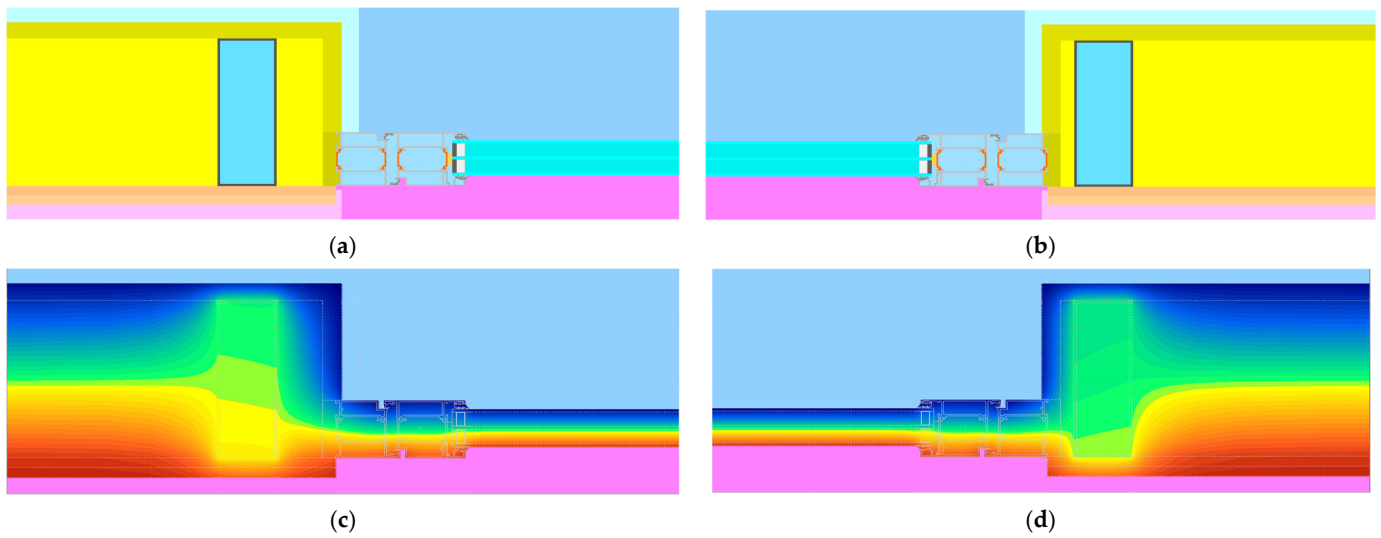

Figure A3. South exterior wall-curtain wall horizontal connection. Geometrical models: (**a**) left margin; (**b**) right margin; Isothermal surfaces: (**c**) left margin; (**d**) right margin.
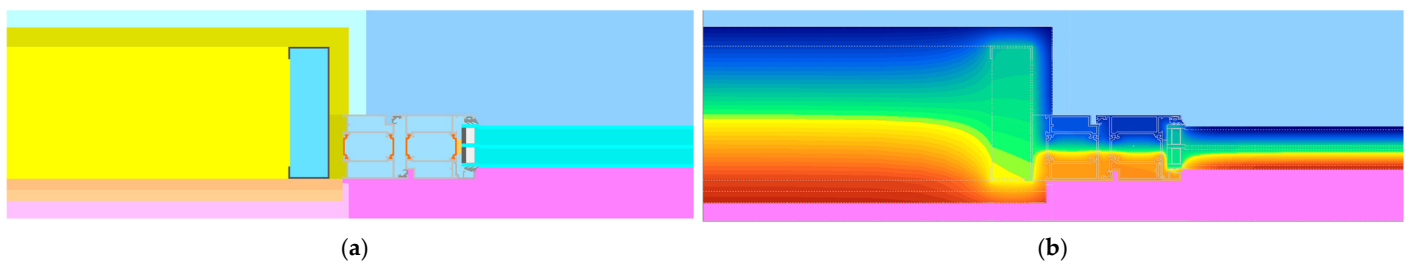

Figure A4. Exterior wall-window horizontal connection: (**a**) Geometrical models; (**b**) Isothermal surfaces.
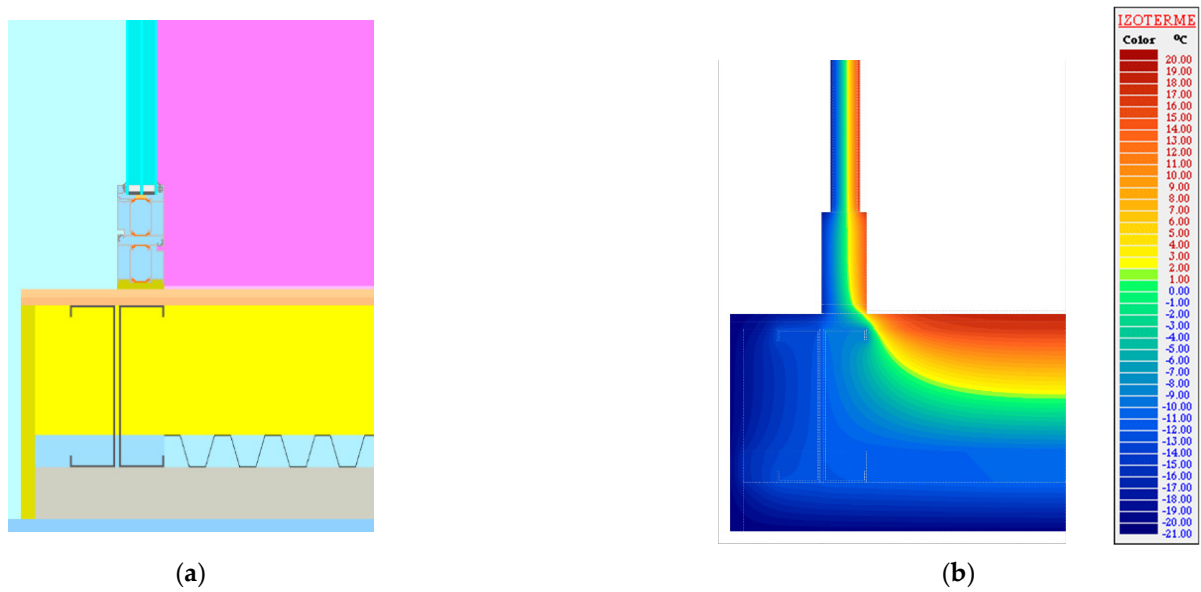
(**a**) (**b**)

Figure A5. Curtain glass-floor in contact with the exterior: (**a**) Geometrical models; (**b**) Isothermal surfaces.

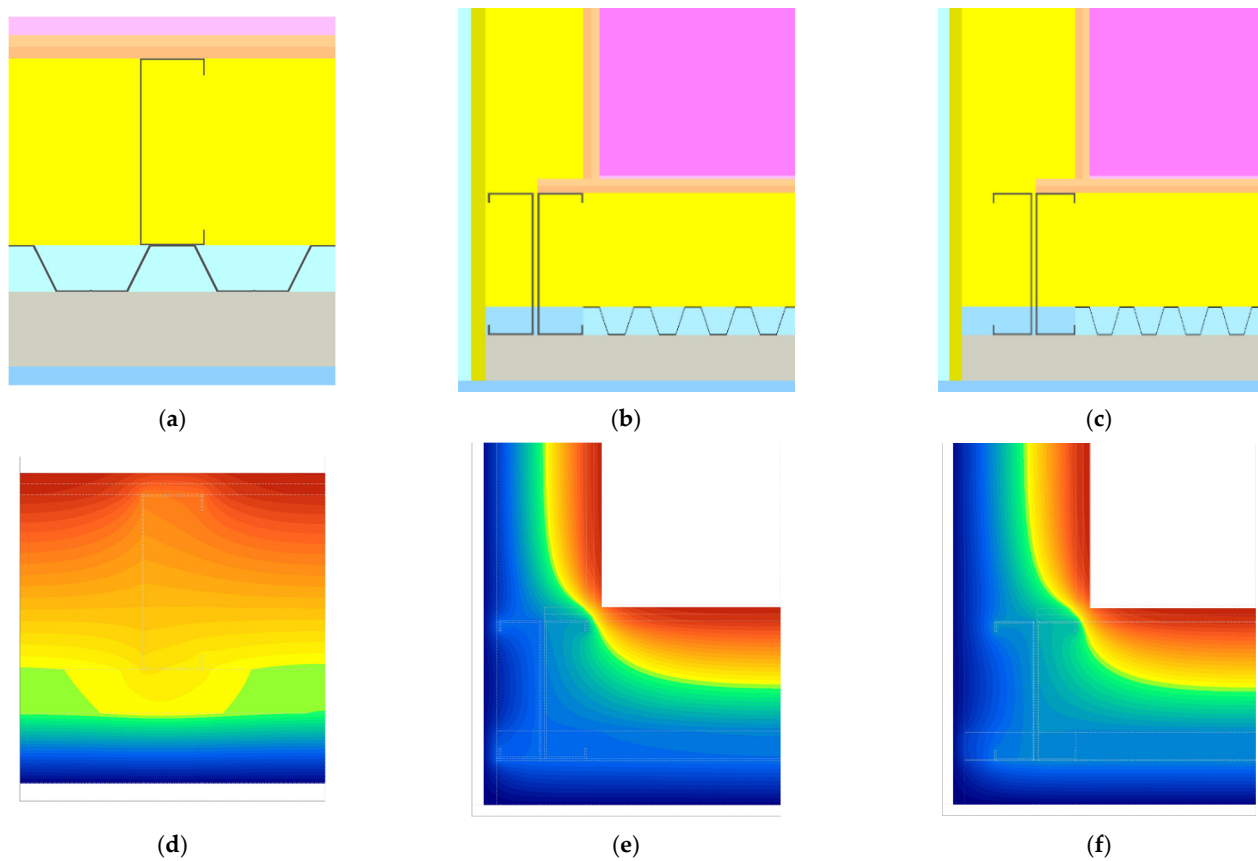(**a**) (**b**) (**c**)

(**d**) (**e**) (**f**)

Figure A6. The floor in contact with the exterior-Geometrical models: (**a**) current field, (**b**) exterior wall (E, W)—floor in contact with the exterior, (**c**) exterior wall (N)—floor in contact with the exterior; Isothermal surfaces (**d**) current field, (**e**) exterior-wall-floor in contact with the exterior, (**f**) exterior wall (N)—floor in contact with the exterior.
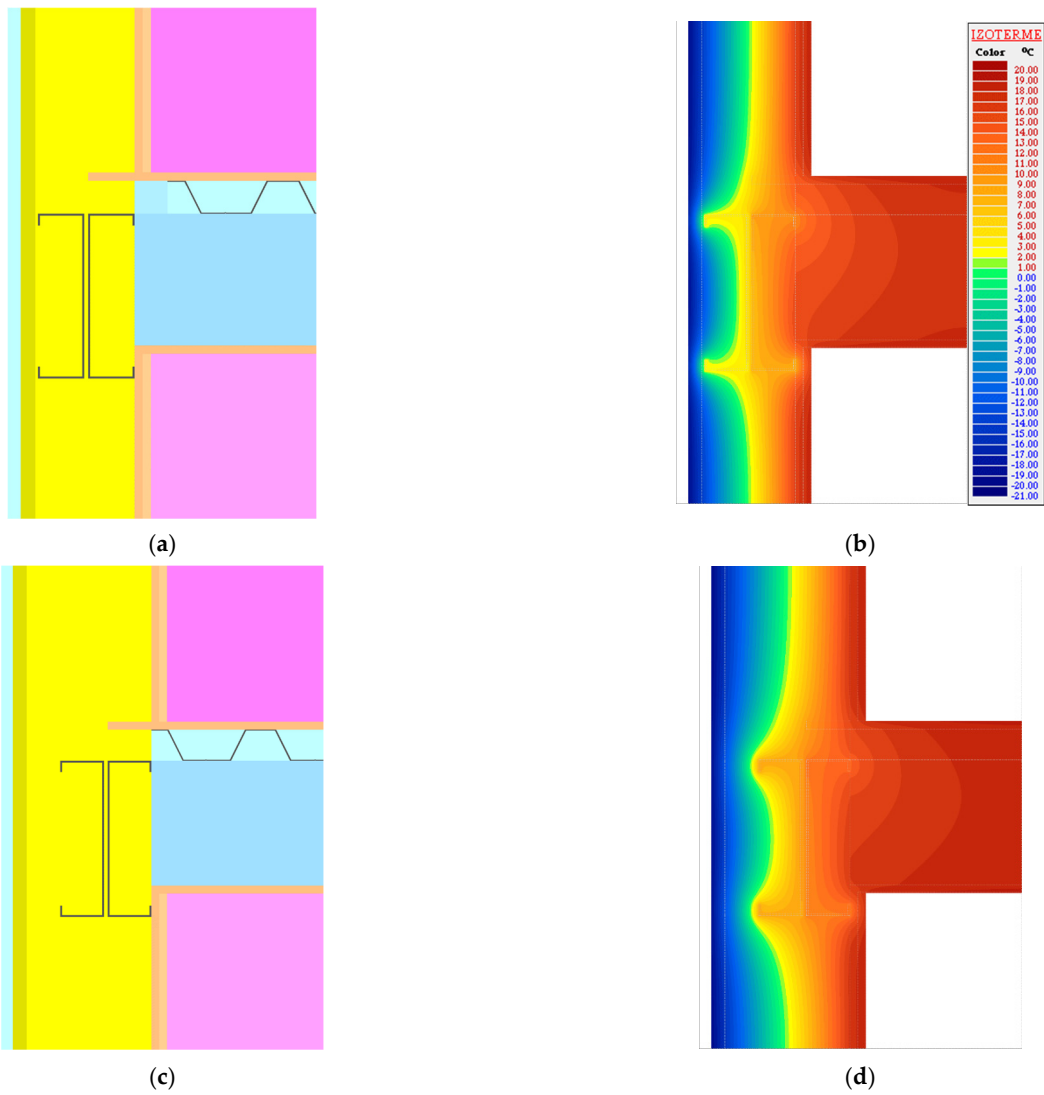
(**a**)

(**b**)

(**c**)

(**d**)

Figure A7. Exterior wall-intermediate floor-Geometrical models (**a**) E-W wall (**c**) N wall; Isothermal surfaces (**b**) E-W wall (**d**) N wall.
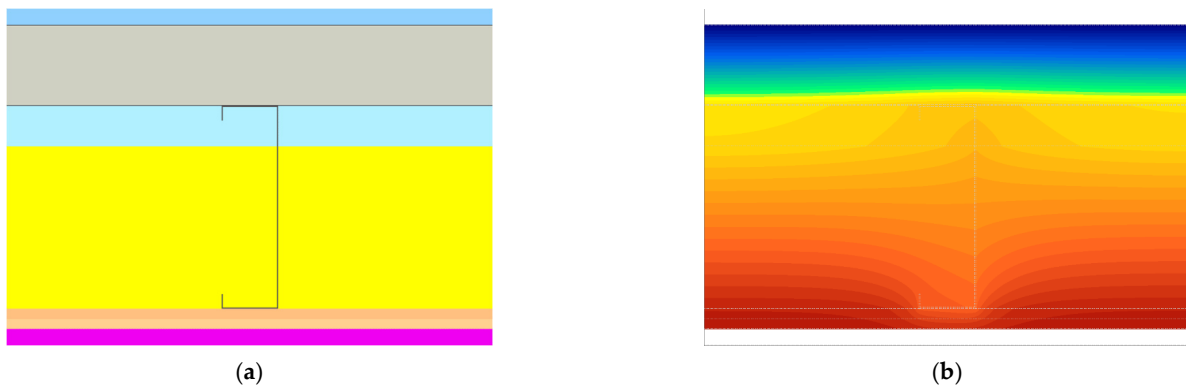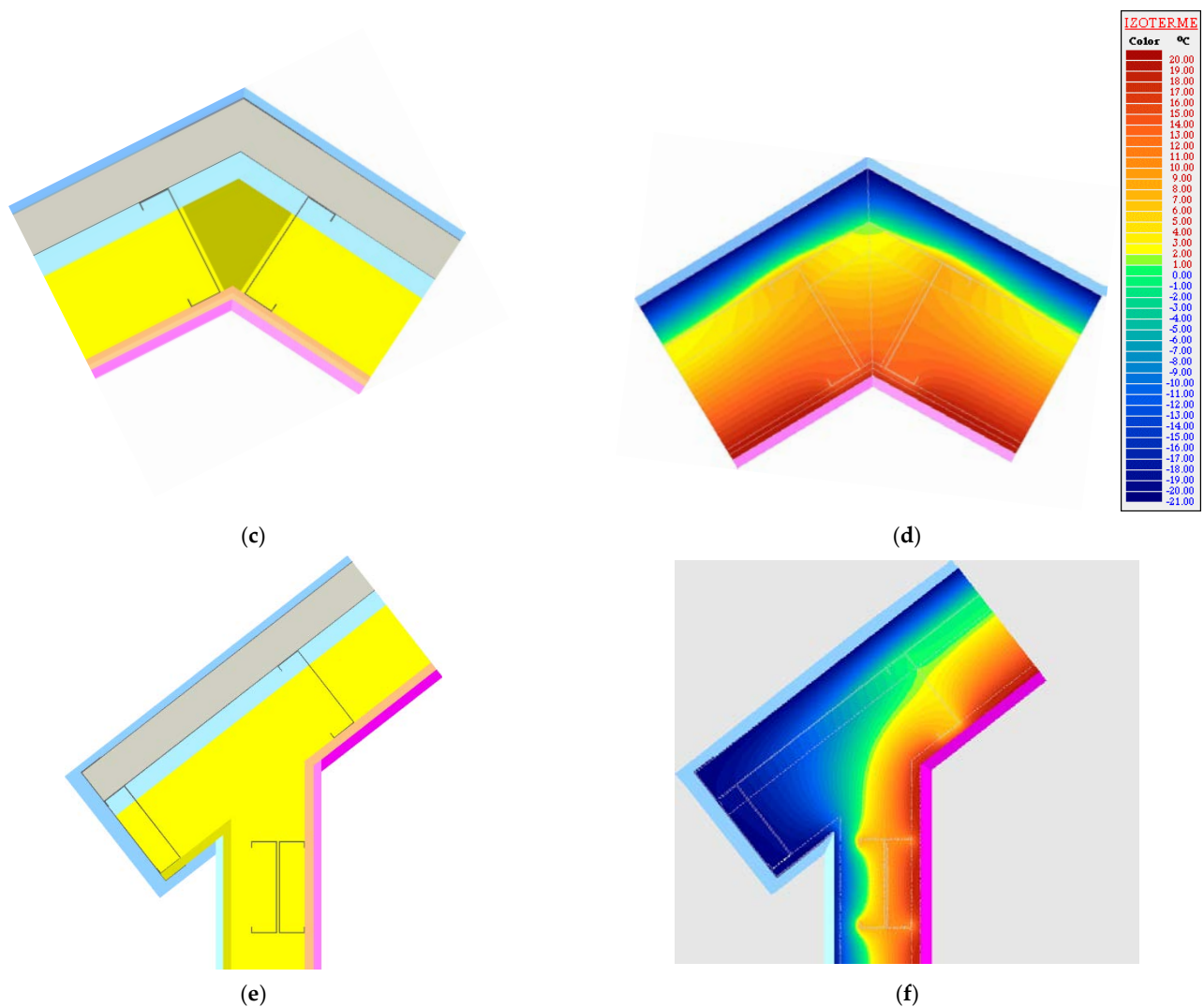

(**a**)

(**b**)

Figure A8. *Cont.*

Figure A8. Roof-Geometrical models (**a**) current field, (**c**) ridge, (**e**) eaves; Isothermal (**b**) current field, (**d**) ridge, (**f**) eaves.

References

1. EU Commission. *In Focus: Energy Efficiency in Buildings*; EU Commission: Brussels, Belgium, 2020.
2. EU Commission. *A European Green Deal. Striving to be the First Climate-Neutral Continent*; EU Commission: Brussels, Belgium, 2020.
3. EU Commission. *Directive (EU) 2018/844 of the European Parliament and of the Council of 30th May 2018 Amending Directive 2010/31/EU on the Energy Performance of Buildings and Directive 2012/27/EU on Energy Efficiency*; EU Commission: Brussels, Belgium, 2018.
4. EU Commission. *National Energy and Climate Plans EU Countries' 10-year National Energy and Climate Plans for 2021–2030*; EU Commission: Brussels, Belgium, 2018.
5. EU Commission. *Directive 2012/27/EU of the European Parliament and of the Council of 25th October 2012 on Energy Efficiency, Amending Directives 2009/125/EC and 2010/30/EU and Repealing Directives 2004/8/EC and 2006/32/ECText with EEA Relevance*; EU Commission: Brussels, Belgium, 2012.
6. EU Commission. *Proposal for a Directive of The European Parliament and of the Council on Energy Efficiency (Recast)*; EU Commission: Brussels, Belgium, 2021.
7. EU Commission. *'Fit for 55': Delivering the EU's 2030 Climate Target on the Way to Climate Neutrality*; EU Commission: Brussels, Belgium, 2021.
8. EU Commission. *An EU-Wide Assessment of National Energy and Climate Plans Driving Forward the Green Transition and Promoting Economic Recovery through Integrated Energy and Climate Planning*; EU Commission: Brussels, Belgium, 2020.
9. International Energy Agency. Energy Efficiency 2019. The Authoritative Tracker of Global Energy Efficiency Trends. 2019. Available online: https://www.iea.org/reports/energy-efficiency-2019 (accessed on 14 October 2021).
10. United Nations Environment Programme. *2020 Global Status Report for Buildings and Construction. Towards a Zero-Emissions, Efficient and Resilient Buildings and Construction Sector*; United Nations Environment Programme: Nairobi, Kenya, 2020.

11. Ürge-Vorsatz, D.; Cabeza, L.F.; Serrano, S.; Barreneche, C.; Petrichenko, K. Heating and cooling energy trends and drivers in buildings. *Renew. Sustain. Energy Rev.* **2015**, *41*, 85–98. [CrossRef]

12. Romanian Ministry of Research and Innovation, CCCDI—UEFISCDI, project number PN-III-P1-1.2-PCCDI-2017-0391/CIA_CLIM–Smart Buildings Adaptable to the Climate Change Effects, within PNCDI III, 2018–2021. Available online: https://www.icer.ro/cercetare/proiecte-de-cercetare/cia-clim (accessed on 14 October 2021).

13. Soares, N.; Santos, P.; Gervásio, H.; Costa, J.J.; Simões da Silva, L. Energy efficiency and thermal performance of lightweight steel-framed (LSF) construction: A review. *Renew. Sustain. Energy Rev.* **2017**, *78*, 194–209. [CrossRef]

14. Santos, P.; Ribeiro, T. Thermal Performance Improvement of Double-Pane Lightweight Steel Framed Walls Using Thermal Break Strips and Reflective Foils. *Energies* **2021**, *14*, 6927. [CrossRef]

15. Rajanayagam, H.; Upasiri, I.; Poologanathan, K.; Gatheeshgar, P.; Sherlock, P.; Konthesingha, C.; Nagaratnam, B.; Perera, D. Thermal Performance of LSF Wall Systems with Vacuum Insulation Panels. *Buildings* **2021**, *11*, 621. [CrossRef]

16. Kempton, L.; Kokogiannakis, G.; Green, A.; Cooper, P. Evaluation of thermal bridging mitigation techniques and impact of calculation methods for lightweight steel frame external wall systems. *J. Build. Eng.* **2021**, *43*, 102893. [CrossRef]

17. Santos, P.; Mateus, D. Experimental assessment of thermal break strips performance in load-bearing and non-load-bearing LSF walls. *J. Build. Eng.* **2020**, *32*, 101693. [CrossRef]

18. Santos, P.; Lemes, G.; Mateus, D. Thermal Transmittance of Internal Partition and External Facade LSF Walls: A Parametric Study. *Energies* **2019**, *12*, 2671. [CrossRef]

19. Ministry of Regional Development. Public Administration and European Funds, Order 2641 regarding the modification and completion of the technical regulation. In *Methodology for Calculating the Energy Performance of Buildings*; Approved by the Order of the Minister of Transport, Construction and Tourism no. 157/2007; Ministry of Regional Development: Bucharest, Romania, 2017.

20. Ministry of Regional Development and Public Administration. Order 386 for the modification and completion of the Technical Regulation. In *Normative Regarding the Thermotechnical Calculation of the Construction Elements of the Buildings*; Indicative C 107-2005; Ministry of Regional Development and Public Administration: Bucharest, Romania, 2016.

21. Ministry of Regional Development and Public Administration. *Indicative Mc001 Part 6 Methodology for Calculating the Energy Performance of Buildings*; Ministry of Regional Development and Public Administration: Bucharest, Romania, 2013.

22. Buzatu, R.; Ungureanu, V.; Ciutina, A.; Gireadă, M.; Vitan, D.; Petran, I. Experimental Evaluation of Energy-Efficiency in a Holistically Designed Building. *Energies* **2021**, *14*, 5061. [CrossRef]

23. Gorgolewski, M. Developing a simplified method of calculating U-values in light steel framing. *Build. Environ.* **2007**, *42*, 230–236. [CrossRef]

24. Santos, P.; Gonçalves, M.; Martins, C.; Soares, N.; Costa, J.J. Thermal transmittance of lightweight steel framed walls: Experimental versus numerical and analytical approaches. *J. Build. Eng.* **2019**, *25*, 100776. [CrossRef]

25. Ciutina, A.; Mirea, M.; Ciopec, A.; Ungureanu, V.; Buzatu, R.; Morovan, R. Behaviour of wedge foundations under axial compression. *IOP Conf. Ser. Earth Environ. Sci.* **2021**, *664*, 012036. [CrossRef]

26. Buzatu, R.; Muntean, D.; Ciutina, A.; Ungureanu, V. Thermal Performance and Energy Efficiency of Lightweight Steel Buildings: A Case-Study. *IOP Conf. Ser. Mater. Sci. Eng.* **2020**, *960*, 032099. [CrossRef]

27. Ciutina, A.; Buzatu, R.; Muntean, D.M.; Ungureanu, V. Heat transfer vs environmental impact of modern façade systems. *E3S Web Conf.* **2019**, *111*, 03078. [CrossRef]

28. Intini, F.; Kühtz, S. Recycling in buildings: An LCA case study of a thermal insulation panel made of polyester fiber, recycled from post-consumer PET bottles. *Int. J. Life Cycle Assess.* **2011**, *16*, 306–315. [CrossRef]

29. *EN ISO 6946*; European Committee for Standardization. Building Components and Building Elements—Thermal Resistance and thermal transmittance—Calculation Methods. CEN: Brussels, Belgium, 2017.

30. de Angelis, E.; Serra, E. Light Steel-frame Walls: Thermal Insulation Performances and Thermal Bridges. *Energy Procedia* **2014**, *45*, 362–371. [CrossRef]

31. C107 Norm for Thermotechnical Calculation of the Construction Elements of Buildings, Bucharest, Romania. 2005. Available online: https://ec.europa.eu/growth/tools-databases/tris/en/index.cfm/search/?trisaction=search.detail&year=2010&num=465&mLang=SV (accessed on 14 October 2021).

32. Santos, P.; Poologanathan, K. The Importance of Stud Flanges Size and Shape on the Thermal Performance of Lightweight Steel Framed Walls. *Sustainability* **2021**, *13*, 3970. [CrossRef]

33. Moga, L.; Moga, I. Considerations on the Thermal Modelling of Insulated Metal Panel Systems. In Proceedings of the International Building Physics Conference, Syracuse, NY, USA, 26 September 2018. [CrossRef]

34. Lupan, L.; Manea, D.; Moga, L. Improving Thermal Performance of the Wall Panels Using Slotted Steel Stud Framing. *Proc. Technol.* **2016**, *22*, 351–357. [CrossRef]

35. *EN ISO 10211*; European Committee for Standardization. Thermal Bridges in Building Construction—Heat Flows and Surface Temperatures—Detailed Calculations. CEN: Brussels, Belgium, 2017.

36. PSIPLAN Software. *Two-Dimensional Heat Transfer for Building Modelling Software for Calculating the Linear Thermal Transmittance Value*; Technical University of Cluj-Napoca: Cluj-Napoca, Romania, 2021.

37. Moga, L.; Moga, I. Evaluation of Thermal Bridges Using Online Simulation Software. *E3S Web Conf.* **2020**, *172*, 08010. [CrossRef]

38. Moga, L. Analytic Study of Thermal Bridges Met at High Performance Energy Efficient Buildings. *Inter. Multidis. Scien. GeoConf. SGEM* **2018**, *18*, 621–626. [CrossRef]

39. Moga, L.; Moga, I. *Specific Thermal Bridges at Load Bearing Masonry Buildings*; UTPRESS: Cluj-Napoca, Romania, 2013.
40. *ISO 13789*; Thermal Performance of Buildings–Transmission and Ventilation Heat Transfer Coefficients—Calculation Method. ISO: Brussels, Belgium, 2015.
41. *ISO 52016-1*; Energy Performance of Buildings—Energy Needs for Heating and Cooling, Internal Temperatures and Sensible and Latent Heat Loads—Part 1: Calculation Procedures. ISO: Brussels, Belgium, 2017.
42. Ubakus—Online U-Wert Calculator. Available online: https://www.ubakus.de/u-wert-rechner/ (accessed on 5 October 2021).
43. Ministry of Transportation. *Constructions and Tourism, Indicative Mc001 Parts 1,2,3 Methodology for Calculating the Energy Performance of Buildings*; Ministry of Transportation: Bucharest, Romania, 2006.
44. Ministry of Development, Public Works and Administration Indicative Mc001 2021 Methodology for Calculating the Energy Performance of Buildings-Updated Version Preprint, Bucharest, Romania. Available online: https://epbd-ca.eu/ca-outcomes/outcomes-2015-2018/book-2018/countries/romania (accessed on 14 October 2021).
45. Vajó, B.; Lakatos, Á. Super Insulation Materials—An Application to Historical Buildings. *Buildings* **2021**, *11*, 525. [CrossRef]
46. Lakatos, Á. Thermophysical investigations of nanotechnological insulation materials. *AIP Conf. Proc.* **2017**, *1866*, 030003. [CrossRef]
47. Lakatos, Á.; Csarnovics, I.; Csík, A. Systematic Analysis of Micro-Fiber Thermal Insulations from a Thermal Properties Point of View. *Appl. Sci.* **2021**, *11*, 4943. [CrossRef]
48. *ISO 13788*; Hygrothermal Performance of Building Components and Building Elements—Internal Surface Temperature to Avoid Critical Surface Humidity and Interstitial Condensation—Calculation Methods. ISO: Brussels, Belgium, 2012.
49. Șoimoșan, T.M.; Moga, L.M.; Anastasiu, L.; Manea, D.L.; Căzilă, A.; Zeljković, Č. Overall Efficiency of On-Site Production and Storage of Solar Thermal Energy. *Sustainability* **2021**, *13*, 1360. [CrossRef]
50. Jack, R. *Building Diagnostics: Practical Measurement of the Fabric Thermal Performance of House*; Figure share; Loughborough University: Loughborough, UK, 2015.